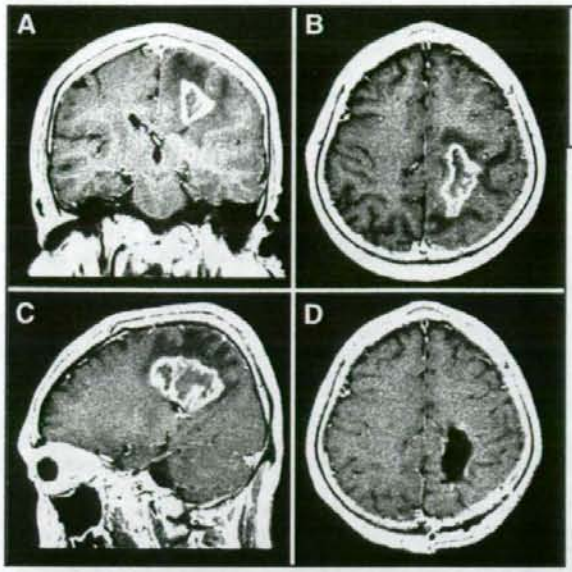

FIGURE 5. *Pre- and postoperative Gd-enhanced, T1-weighted MRI scans of Patient 3.* A–C, *preoperative Gd-enhanced, T1-weighted coronal* (A), *axial* (B), *and sagittal* (C) *images. Ring-like enhancement with perifocal edema was observed in each image.* D, *Gd-enhanced, T1-weighted MRI scan obtained 2 months after the operation.*

improved and he recovered his ability to walk 1 week after the operation with a decrease in perifocal edema (data not shown).

Patient 3

A 42-year old man was introduced to our clinic with a left parietal mass with ring-enhancement by Gd administration, as indicated on MRI scans (*Fig. 5, A–C*). He experienced right hemiparesis and hemisensory disturbance on admission. The preoperative diagnosis was glioblastoma based on this MRI scan. We performed a left frontoparietal craniotomy with 5-ALA guidance. The excitation for the PpIX in this case was done by a high-power violet laser light. After the cortical incision, the mass was observed with the aid of this excitation system. Some parts of the lesion showed strong red fluorescence (*Fig. 6B*) and some parts showed only a relatively green autofluorescence (*Fig. 6A*). A rapid intraoperative diagnosis from a frozen specimen was uncertain. Hematoxylin and eosin (H & E) staining from the fluorescence-negative lesion showed typical necrosis (*Fig. 6A*), whereas that from strong fluorescence-positive areas showed cellular infiltration in

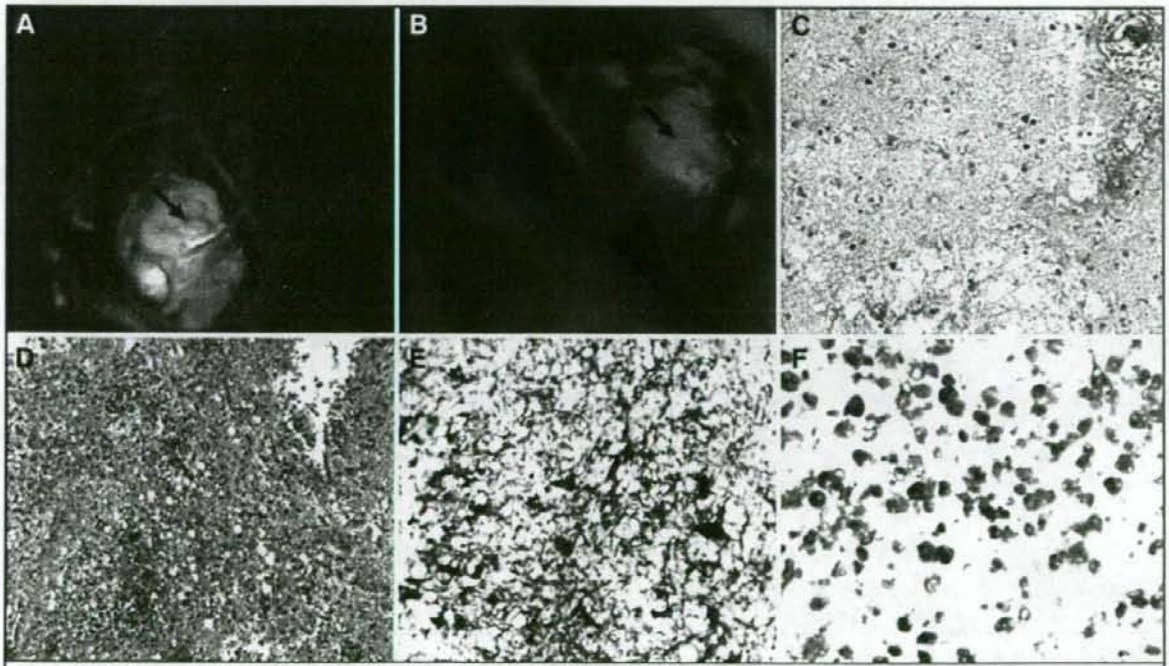

FIGURE 6. *Intraoperative photographs showing histopathological and immunohistochemical findings in Patient 3.* A *and* B, *dark-field intraoperative photographs with high-power violet laser excitation.* C, *H & E staining of a fluorescence-negative area, which is identical to that indicated by the* black arrow. D, *H & E staining of a fluorescence-positive area, which is identical with that indicated by the* black arrow. *Marked cell infiltration was seen.* E *and* F, *immunohistochemical analysis with anti-GFAP and anti-KP-1 antibodies of the same sample of* B. *Original magnification,* ×5 (C *and* D) *and* ×10 (E *and* F).

the white matter (*Fig. 6B*). Some parts of the specimen showed perivascular lymphocyte cuffing (data not shown). Immunohistochemical study with anti-GFAP and anti-macrophage antibodies (KP-1) revealed many reactive astrocytes and macrophages in the infiltrative cell zone. Luxol fast blue staining revealed that some macrophages phagocyted fragmented myelin sheath (data not shown). No obvious tumor cells could be identified from any of the surgical specimens. Taken together, the most probable diagnosis was acute multiple sclerosis, although the lesion was not multiple in time and space, and no enhanced lesion appeared during the follow-up period (*Fig. 5D*). Some neurologists gave us the possibility of Neuro-Behcet's syndrome from the high value of the interleukin-6 in the cerebrospinal fluid (3).

DISCUSSION

We introduce two nontumorous pathological conditions in which PpIX fluorescence activity was observed by 5-ALA administration, one being pure radiation necrosis without tumor recurrence and the other being neurodegenerative demyelinating disease. In our preliminary experiments using the cold injury model in rodents, fluorescent activity of PpIX was observed in the lesions with 5-ALA administration (data not shown). It remains unclear which cells express this fluorescence. There is also the possibility that some PpIX produced elsewhere in the body is transferred to these areas, although using high-performance liquid chromatography in these experiments, we could detect only the scarce activity of PpIX in the serum of the animals administered 5-ALA (data not shown). In the experiments, at least, the breakdown of the blood-brain barrier (BBB) is essential for the expression of this fluorescence activity; this breakdown was confirmed by the administration of Evans blue dye (data not shown).

Although the breakdown of the BBB is essential for the expression of PpIX red fluorescence activity, we do not speculate that only the breakdown of the BBB is the cause of PpIX fluorescence activity. As Stummer et al. (16) report, some malignant gliomas do not show PpIX fluorescence even though they show Gd enhancement on MRI scans. Recently, we reported that PpIX fluorescence can be identified in some meningiomas but cannot be identified in other meningiomas even though they show Gd enhancement on MRI scans (4). Additionally, many metastatic brain tumors with Gd enhancement on MRI scans do not show any PpIX fluorescence (unpublished data). In our rat cold injury model and by observation in human tumors, we could not identify the distinctive PpIX fluorescence activity in the choroid plexus by our detection system (data not shown). Thus, it is safe to assume that some other condition is necessary in addition to the breakdown of the BBB for PpIX activity, although the exact other condition remains unknown.

At first, we speculate that cell proliferation may be essential for the expression of PpIX activity around the perinecrotic lesion. In the human cases mentioned here, less than 1% of infiltrative cells were stained with Ki-67 antibody, which may refute this speculation (data not shown). In animal studies, we were able to observe some perilesional reactive astrocytes and inflammatory cell infiltration around the fluorescence positive area (data not shown). These observations are consistent with our findings in the present human cases. In the literature on radiation necrosis, reactive astrocytes and macrophage infiltration are commonly observed between the necrotic center and the surrounding brain (H Takeshima, personal communication) (17, 18).

In radiation necrosis, we observed relatively weak (vague) fluorescence. In the perinecrotic area in neurodegenerative disease in Patient 3, we observed vivid red fluorescence, which was believed to be a malignant glioma during the operation. Marked cell infiltration, including reactive astrocytes and macrophages, was observed in this case. There was also an increase of interleukin-6 in the cerebrospinal fluid, suggesting inflammation (3). These conditions might produce strong fluorescence. With respect to dysplasia status in the bladder, the fluorescence activity of PpIX can be observed by the administration of 5-ALA (7). This also supports our present observations. For further analysis, it is necessary to develop an appropriate fixation method for PpIX in vivo or to develop a good antibody to detect PpIX which would be applicable in double staining, such as with anti-GFAP or anti-macrophage antibodies. In any case, it is important to keep in mind that fluorescence-positive tissue in the brain is not always tumorous. Finally, let us stress that fluorescence-guided surgery for the removal of necrotic tissue is a highly useful technique.

CONCLUSION

In conclusion, BBB alteration is necessary, but not sufficient, for PpIX red fluorescence; Gd-enhancing lesions may be fluorescent, even if there is no tumor present; and although not new, these cases underscore the need for surgical caution when using 5-ALA for surgical guidance.

REFERENCES

1. Baumgartner R, Huber RM, Schulz H, Stepp H, Rick K, Gamarra F, Leberig A, Roth C: Inhalation of 5-aminolevulinic acid: A new technique for fluorescence detection of early stage lung cancer. **J Photochem Photobiol B** 36:169–174, 1996.
2. Ennis SR, Novotny A, Xiang J, Shakui P, Masada T, Stummer W, Smith DE, Keep RF: Transport of 5-aminolevulinic acid between blood and brain. **Brain Res** 959:226–234, 2003.
3. Hirohata S, Isshi K, Oguchi H, Ohse T, Haraoka H, Takeuchi A, Hashimoto H: Cerebrospinal fluid interleukin-6 in progressive Neuro-Behcet's syndrome. **Clin Immunol Immunopathol** 82:12–17, 1997.
4. Kajimoto Y, Kuroiwa T, Miyatake S, Ichioka T, Miyashita M, Tanaka H, Tsuji M: Use of 5-aminolevulinic acid in fluorescence-guided resection of meningioma with high risk of recurrence. Case report. **J Neurosurg** 106:1070–1074, 2007.
5. Kawabata S, Miyatake S, Kajimoto Y, Kuroda Y, Kuroiwa T, Imahori I, Kirihata M, Sakurai Y, Kobayashi T, Ono K: The early successful treatment of glioblastoma patients with modified boron neutron capture therapy. Report of two cases. **J Neurooncol** 65:159–165, 2003.
6. Kriegmair M, Baumgartner R, Knuchel R, Stepp H, Hofstadter F, Hofstetter A: Detection of early bladder cancer by 5-aminolevulinic acid induced porphyrin fluorescence. **J Urol** 155:105–110, 1996.
7. Landry JL, Gelet A, Bouvier R, Dubernard JM, Martin X, Colombel M: Detection of bladder dysplasia using 5-aminolevulinic acid-induced porphyrin fluorescence. **BJU Int** 91:623–626, 2003.
8. Lange N, Jichlinski P, Zellweger M, Forrer M, Marti A, Guillou L, Kucera P, Wagnieres G, van den Bergh H: Photodetection of early human bladder can-

cer based on the fluorescence of 5-aminolaevulinic acid hexylester-induced protoporphyrin IX: A pilot study. **Br J Cancer** 80:185–193, 1999.
9. Miyatake S, Kawabata S, Kajimoto Y, Aoki A, Yokoyama K, Yamada M, Kuroiwa T, Tsuji M, Imahori Y, Kirihata M, Sakurai Y, Masunaga S, Nagata K, Maruhashi A, Ono K: Modified boron neutron capture therapy for malignant gliomas performed using epithermal neutron and two boron compounds with different accumulation mechanisms: An efficacy study based on findings on neuroimages. **J Neurosurg** 103:1000–1009, 2005.
10. Monnier P, Savary M, Fontolliet C, Wagnieres G, Chatelain A, Cornaz P, Depeursinge C, Van Den Bergh H: Photodetection and photodynamic therapy of early squamous cell carcinomas of the pharynx, esophagus and tracheobronchial tree. **Lasers Med Sci** 5:149–169, 1990.
11. Olivo M, Wilson BC: Mapping ALA-induced PPIX fluorescence in normal brain and brain tumour using confocal fluorescence microscopy. **Int J Oncol** 25:37–45, 2004.
12. Peng Q, Warloe T, Berg K, Moan J, Kongshaug M, Giercksky KE, Nesland JM: 5-Aminolevulinic acid-based photodynamic therapy. Clinical research and future challenges. **Cancer** 79:2282–2308, 1997.
13. Stummer W, Novotny A, Stepp H, Goetz C, Bise K, Reulen HJ: Fluorescence-guided resection of glioblastoma multiforme by using 5-aminolevulinic acid-induced porphyrins: A prospective study in 52 consecutive patients. **J Neurosurg** 93:1003–1013, 2000.
14. Stummer W, Pichlmeier U, Meinel T, Wiestler OD, Zanella F, Reulen HJ; ALA-Glioma Study Group: Fluorescence-guided surgery with 5-aminolevulinic acid for resection of malignant glioma: A randomised controlled multicentre phase III trial. **Lancet Oncol** 7:392–401, 2006.
15. Stummer W, Reulen HJ, Novotny A, Stepp H, Tonn JC: Fluorescence-guided resections of malignant gliomas—an overview. **Acta Neurochir Suppl** 88:9–12, 2003.
16. Stummer W, Stocker S, Wagner S, Stepp H, Fritsch C, Goetz C, Goetz AE, Kiefmann R, Reulen HJ: Intraoperative detection of malignant gliomas by 5-aminolevulinic acid-induced porphyrin fluorescence. **Neurosurgery** 42: 518–526, 1998.
17. Tsuyuguchi N, Tamaki T, Sunada I, Iwai Y, Yamanaka K, Tanaka K, Nishikawa M, Ohata K, Torii K, Morino M, Nishio A, Hara M: Methionine positron emission tomography for differentiation of recurrent brain tumor and radiation necrosis after stereotactic radiosurgery—In malignant glioma. **Ann Nucl Med** 18:291–296, 2004.
18. Yang T, Wu SL, Liang JC, Rao ZR, Ju G: Time-dependent astroglial changes after gamma knife radiosurgery in the rat forebrain. **Neurosurgery** 47: 407–416, 2000.

Acknowledgments

We thank Hideo Takeshima, M.D., Ph.D., Department of Neurosurgery, Miyazaki University, Miyazaki, Japan for the information about macrophage infiltration in radiation necrosis. This work was partly supported by a Grant-in-Aid for Exploratory Research (16659396) to Toshihiko Kuroiwa, M.D., and Scientific Research (C) (17591357) to Yoshinaga Kajimoto, M.D., from the Japanese Ministry of Education, Science, and Culture.

COMMENTS

In this report, Miyatake et al. present three patients with enhancing lesions on imaging for which 5-ALA was used to guide resection margins. The conclusions from this small series highlight an important admonition for any surgeon performing fluorescence-guided resections: 5-ALA can enhance other pathological tissues, including demyelination and radiation-induced necrosis. Given the current opinions that 5-ALA is very specific (up to 100% specificity in one report which looked at biopsy specimens [1]), the observation of these authors is especially important. 5-ALA is currently in limited use in the United States and Europe; 5-ALA is not approved by the United States Food and Drug Administration for use in brain tumor surgery.

The authors correctly cite the study by Olivo and Wilson (2), which showed that 5-ALA crosses the blood brain barrier (BBB) and choroid plexus with the majority of PpIX accumulation (the fluorescent metabolite of 5-ALA) occurring in tumors. There was another important observation in this report, namely that areas of acute inflammation within the brain also accumulate PpIX. Radiation necrosis and demyelination certainly contain areas of, and are likely caused by, inflammation, and inflammation may be the sole confounding issue with respect to non-tumor PpIX accumulation in this series. One could hypothesize that hypermetabolic cells in general will metabolize 5-ALA to PpIX.

Demyelination and radiation necrosis are typically in the differential for any enhancing, edematous lesion on magnetic resonance imaging, depending on the context. Once one commits a patient to a resection, the fact that 5-ALA fluorescence may occur in nonmalignant, abnormal tissue should not limit its use. Instead, we should focus on the specificity of this marker for pathological tissue, potentially improving resection margins where patient safety permits.

Michael L. DiLuna
Joseph M. Piepmeier
New Haven, Connecticut

---

1. Stummer W, Stocker S, Wagner S, Stepp H, Fritsch C, Goetz C, Goetz AE, Kiefmann R, Reulen HJ: Intraoperative detection of malignant gliomas by 5-aminolevulinic acid-induced porphyrin fluorescence. **Neurosurgery** 42:518–526, 1998.
2. Olivo M, Wilson BC: Mapping ALA-induced PPIX fluorescence in normal brain and brain tumour using confocal fluorescence microscopy. **Int J Oncol** 25:37–45, 2004.

This report presents a cautionary series of three cases that serve to highlight the fact that not all gadolinium-enhancing or 5-ALA-fluorescing lesions are tumors. This should serve as a warning that resecting tissue that demonstrates 5-ALA fluorescence may not ensure the neurosurgeon that he is in neoplastic tissue. 5-ALA, which has been used to facilitate malignant glioma resection, was used to guide resection of two cases of radiation necrosis after boron neutron capture therapy and one case of inflammatory demyelinating disease. This report corroborates the fact that 5-ALA can be found in any area of BBB breakdown. All three lesions enhanced after gadolinium administration, indicating the presence of BBB alteration. The authors further demonstrated that BBB alteration is necessary, but not sufficient, for 5-ALA red fluorescence. Using a rodent head injury model, there was 5-ALA fluorescence after injury. However, some enhancing gliomas and choroid plexus do not fluoresce after 5-ALA administration. Although 5-ALA may lead to a more complete resection of malignant gliomas, care needs to be exercised when relying on this technique.

Daniel L. Silbergeld
Seattle, Washington

Fluorescence-guided resection of gliomas using 5-ALA is gaining increasing popularity as it is thought that it will result in a more rigorous resection of the tumor with preservation of normal brain. Although there is no conclusive evidence that the extent of resection of glioma correlates with improved outcome, there have been numerous studies in both high- and low-grade tumors suggesting the benefit of maximal resection (1). This study clearly documents a valid concern that all that fluoresces may not be a tumor, and fluorescent tissue can certainly be found in oedematous brain that may be infiltrated by tumor cells but also in radionecrosis and demyelination as reported by the authors. Porphyrin sensitisers such as 5-ALA are known to accumulate in tissue not protected by the BBB (2).

Although the use of 5-ALA may improve the extent of resection, care must be taken that the eloquent brain, which is oedematous and infiltrated by a tumor but is still functional, should not be resected even though it may fluoresce. A radical resection of a high-grade glioma does not provide a cure, and it is critical that surgery should not result in a serious morbidity.

Andrew H. Kaye
Melbourne, Australia

1. Walker DG, Kaye AH: Low grade glial neoplasms. **J Clin Neurosci** 10:1–13, 2003.
2. Stylli SS, Kaye AH: Photodynamic therapy of cerebral glioma–A review. Part I–A biological basis. **J Clin Neurosci** 13: 615–625, 2006.

The authors report on a few cases where 5-aminolevulenic acid (5-ALA) provides intraoperative visualization in some non-neoplastic disorders. This report emphasizes the emerging role of this agent as a surgical adjunct and is a harbinger of things to come as other intraoperative "contrast agents" emerge to assist the surgeon at surgery. These agents, particularly in conjunction with navigation systems, may prove to allow better, safer surgical resection of brain lesions and may obviate the need for intraoperative imaging, particularly when reliable intraoperative methods of visualizing low-grade gliomas become available.

Gene H. Barnett
Cleveland, Ohio

Interaction of Arginine-Rich Peptides with Membrane-Associated Proteoglycans Is Crucial for Induction of Actin Organization and Macropinocytosis†

Ikuhiko Nakase,[‡,§] Akiko Tadokoro,[§,∥] Noriko Kawabata,[‡] Toshihide Takeuchi,[‡] Hironori Katoh,[⊥] Kiyo Hiramoto,[⊥] Manabu Negishi,[⊥] Motoyoshi Nomizu,[#] Yukio Sugiura,[‡] and Shiroh Futaki*[,‡,∥]

Institute for Chemical Research, Kyoto University, Uji, Kyoto 611-0011, Japan, Graduate School of Biostudies, Kyoto University, Sakyo-ku, Kyoto 606-8501, Japan, School of Pharmacy, Tokyo University of Pharmacy and Life Science, Hachioji, Tokyo 192-0392, Japan, and SORST, Japan Science and Technology Agency, Kawaguchi, Saitama 332-0012, Japan

Received June 26, 2006; Revised Manuscript Received September 20, 2006

ABSTRACT: Arginine-rich peptides, including octaarginine (R8), HIV-1 Tat, and branched-chain arginine-rich peptides, belong to one of the major classes of cell-permeable peptides which deliver various proteins and macromolecules to cells. The importance of the endocytic pathways has recently been demonstrated in the cellular uptake of these peptides. We have previously shown that macropinocytosis is one of the major pathways for cellular uptake and that organization of the F-actin accompanies this process. In this study, using proteoglycan-deficient CHO cells, we have demonstrated that the membrane-associated proteoglycans are indispensable for the induction of the actin organization and the macropinocytic uptake of the arginine-rich peptides. We have also demonstrated that the cellular uptake of the Tat peptide is highly dependent on heparan sulfate proteoglycan (HSPG), whereas the R8 peptide uptake is less dependent on HSPG. This suggests that the structure of the peptides may determine the specificity for HSPG, and that HSPG is not the sole receptor for macropinocytosis. Comparison of the HSPG specificity of the branched-chain arginine-rich peptides in cellular uptake has suggested that the charge density of the peptides may determine the specificity. The activation of the Rac protein and organization of the actin were observed within a few minutes after the peptide treatment. These data strongly suggest the possibility that the interaction of the arginine-rich peptides with the membrane-associated proteoglycans quickly activates the intracellular signals and induces actin organization and macropinocytotis.

Short basic peptide segments derived from HIV-1[1] Tat and Antennapedia homeodomain proteins translocate through cell membranes (*1*−*5*). These peptide segments bind to proteins resulting in the successful uptake of these exogenous molecules into cells, and the cellular responses (*3*, *5*). This suggests the possibility of the pharmaceutical and therapeutic application of this methodology. This efficient internalization pathway has been gaining substantial attraction for the rational design of highly efficient and effective delivery systems. Various arginine-rich peptides or guanidinium-rich derivatives have been shown to have a similar ability (*6*−*11*).

Endocytosis is one of the major pathways for the cellular uptake of proteins. However, the internalization of basic peptides has previously been shown to employ a system other than endocytosis. Endocytosis is an energy dependent pathway and usually suppressed at a low temperature. A highly efficient internalization of basic peptides, comparable to that at 37 °C, was observed even when the cells were treated with the peptides at 4 °C. Microscopic observation of a diffuse cytosolic distribution without punctate, endosome-like compartments and nuclear accumulation of the fluorescently labeled peptides also suggested this hypothesis. It has recently been reported that the fixation previously employed for the microscopic analysis of the peptide internalization can yield a considerable artifact (*12*). Using live cells without fixation has revealed the presence of endosome-like punctate structures in the cytosol, and a significant decrease in the cellular uptake efficiency at 4 °C. These facts strongly suggest active endocytosis of the arginine-rich peptides and their conjugates (*12*).

Macropinocytosis is one of the major pathways for the endocytic uptake of the arginine-rich peptides as well as their

† This work was supported in part by Grants-in-Aid for Scientific Research from the Ministry of Education, Culture, Sports, Science and Technology of Japan. T.T. is grateful for the JSPS Research Fellowship for Young Scientists.

* Corresponding author. Institute for Chemical Research, Kyoto University, Uji, Kyoto 611-0011, Japan. Tel: +81-774-38-3210. Fax: +81-774-32-3038. E-mail: futaki@scl.kyoto-u.ac.jp.

‡ Institute for Chemical Research, Kyoto University.

§ These authors contributed equally to this study.

∥ SORST, Japan Science and Technology Agency.

⊥ Graduate School of Biostudies, Kyoto University.

Tokyo University of Pharmacy and Life Science.

[1] Abbreviations: HIV-1, human immunodeficiency virus type 1; EGF, epidermal growth factor; PDGF, platelet-derived growth factor; FGF, fibroblast growth factor; VEGF, vascular endothelial growth factor; HSPG, heparan sulfate proteoglycan; GAG, glycosaminoglycan; BSA, bovine serum albumin; GST-CRIB, Cdc42/Rac interactive binding motif protein tagged with glutathione S-transferase; CHO, Chinese hamster ovary; ATCC, American Type Culture Collection; DMEM, Dulbecco's modified Eagle medium; α-MEM, α-minimum essential medium; EIPA, 5-(*N*-ethyl-*N*-isopropyl)amiloride; Fmoc, 9-fluorenylmethyloxycarbonyl; TRITC, tetramethylrhodamine isothiocyanate; HPLC, high-performance liquid chromatography; MALDI-TOFMS, matrix-assisted laser desorption ionization time-of-flight mass spectrometry; SDS−PAGE, sodium dodecyl sulfate−polyacrylamide gel electrophoresis.

10.1021/bi0612824 CCC: $37.00 © 2007 American Chemical Society
Published on Web 12/16/2006

protein conjugate (*13*−*15*). Macropinocytosis is different from clathrin-mediated endocytosis which starts with the formation of concave clathrin-coated pits on the plasma membrane. Macropinocytosis involves an actin-driven membrane protrusion and the subsequent fusion with the plasma membrane that engulfs substantial amounts of extracellular fluid as macropinosomes (*16*−*19*). These processes cause the membrane ruffling. Membrane ruffles can be transiently induced in most cells by treatment with the epidermal growth factor (EGF) and platelet-derived growth factor (PDGF) (*17*, *18*). We have already observed that these organizations of F-actin were induced in cells treated with oligoarginine peptides (*13*). Thus, we hypothesize that there are potential receptors for the arginine peptides that induce macropinocytosis together with F-actin organization.

It has been reported that membrane-associated proteoglycans, such as heparan sulfate proteoglycan (HSPG), play a crucial role in the cellular uptake of arginine-rich peptides (*20*−*24*) as well as the 86-residue full length HIV-1 Tat protein (*25*−*28*). A deficiency in HSPG often results in a decrease in the amount of these peptides taken up by the cells. HSPG has been suggested as a primary receptor for the cellular uptake of the arginine-rich peptides. However, the relationship between the interaction of the peptides with HSPG and other membrane-associated proteoglycans and the induction of macropinocytosis has not been established. In addition, the expression of HSPG differs in various tissues, including cancer cells, and thus, HSPG has been regarded as a promising target for drug delivery (*29*, *30*). Studies on the relationship of the macropinocytic uptake of arginine-rich peptides with HSPG should provide valuable information on the design of delivery systems using arginine-rich peptides.

In this report, we show that the structures and the charge densities of the arginine-rich peptides, including the branched-chain peptides, determine their cellular uptake dependency on the membrane-associated proteoglycans, especially HSPG. We also demonstrate that the treatment of the cells with arginine-rich peptides leads to the activation of the Rac protein to induce the F-actin organization and lamellipodia. Most importantly, we find that membrane-associated proteoglycans play a crucial role in the induction of the F-actin organization and macropinocytosis, suggesting that the membrane-associated proteoglycans function as potential receptors for the induction of macropinocytosis by the arginine-rich peptides.

EXPERIMENTAL PROCEDURES

Peptide Synthesis and Fluorescent Labeling. All of the peptides used were chemically synthesized by Fmoc (9-fluorenylmethyloxycarbonyl) solid-phase peptide synthesis on a Rink amide resin as already reported (*13*). The amino acid derivatives and Rink amide resin were purchased from Novabiochem. Deprotection of the peptide and cleavage from the resin were conducted by treatment with a trifluoroacetic acid/ethanedithiol mixture (95:5) at room temperature for 3 h. Fluorescent labeling of the peptides was conducted by treatment with 1.5 equiv of Alexa 488 C_5 maleimide sodium salt (Molecular Probes) in a dimethylformamide/methanol mixture (1:1) for 1.5 h followed by reversed-phase high-performance liquid chromatography (HPLC) purification. The fidelity of the products was ascertained by matrix-assisted laser desorption ionization time-of-flight mass spectrometry (MALDI-TOFMS). MALDI-TOFMS for R8-Alexa, Tat-Alexa, (R2)4-Alexa, (RG3R)4-Alexa, (R1)8-Alexa, R8 (nonlabeled, Arg-Arg-Arg-Arg-Arg-Arg-Arg-Arg-amide), and Tat (nonlabeled, Gly-Arg-Lys-Lys-Arg-Arg-Gln-Arg-Arg-Arg-Pro-Pro-Gln-amide): 2126.2 [expected for $(M + H)^+$ 2125.4]; 2520.7 [expected for $(M + H)^+$ 2520.9]; 2510.4 [expected for $(M + H)^+$ 2509.9]; 3194.2 [expected for $(M + H)^+$ 3194.6]; 3024.6 [expected for $(M + H)^+$ 3023.6], 1267.6 [expected for $(M + H)^+$ 1267.5]; 1718.8 [expected for $(M + H)^+$ 1719.1], respectively.

Cell Culture. Chinese hamster ovary (CHO) cells (CHO-K1 cell lines: wild type; pgsA-745 (A-745) cell lines, all glycosaminoglycan deficient; pgsD-677 (D-677), heparan sulfate deficient) were purchased from the American Type Culture Collection (ATCC) and maintained in F-12 nutrient mixture (Ham's F-12) (Invitrogen) with 10% heat-inactivated fetal bovine serum. The 293T human renal epithelial cells were cultured in Dulbecco's modified Eagle medium (DMEM) with 10% heat-inactivated fetal bovine serum, 2 mM glutamine, 100 units/mL penicillin, and 100 μg/mL streptomycin. The 293T cells stably overexpressing syndecan-2 (*31*) were maintained in the presence of 0.4 μg/mL puromycin. The human cervical cancer-derived HeLa cells were maintained in α-minimum essential medium (α-MEM) with 10% heat-inactivated calf serum. Cells were grown on 100 mm dishes and incubated at 37 °C under 5% CO_2 to approximately 70% confluence. A subculture was performed every 3−4 days.

Confocal Microscopy of Peptide Internalization. CHO cells (2×10^5) were plated on 35 mm glass-bottomed dishes (Iwaki) and cultured in Ham's F-12 with 10% heat-inactivated fetal bovine serum for 48 h. After complete adhesion, the culture medium was exchanged, and then the cells were incubated at 37 °C with fresh medium (200 μL) containing the fluorescently labeled peptides and washed with phosphate buffered saline (PBS) (×3). Distribution of the fluorescently labeled peptides was then analyzed using a confocal scanning laser microscope FV300 (Olympus) equipped with a 40× objective *without fixing* the cells to avoid artifactual localization of the internalized peptides (*12*, *13*).

Flow Cytometry. CHO cells (1.5×10^5) in fresh culture medium (1 mL) were plated into 24-well microplates (Iwaki) and cultured for 48 h in Ham's F-12 containing 10% heat-inactivated fetal bovine serum. After complete adhesion, the cells were incubated at 37 °C for 30 min with fresh medium (200 μL) containing peptides prior to washing with PBS. The cells were then treated with 0.01% trypsin in PBS (200 μL) at 37 °C for 10 min prior to the addition of PBS (200 μL). The cells were centrifuged at 2000 rpm (400*g*) for 5 min. After the supernate was removed, the cells were washed with 500 μL of PBS and centrifuged at 2000 rpm for 5 min. After this washing cycle was repeated, the cells were suspended in PBS (400 μL) and subjected to fluorescence analysis on a FACScalibur (BD Biosciences) flow cytometer using 488 nm laser excitation and a 515 to 545 nm emission filter. Three additional cell washes in the presence of 4 mg/mL heparin in PBS after the trypsinization did not yield any significant difference in the FACS analysis (data not shown). In addition, we confirmed that the cell surface proteoglycans

were effectively removed by the above trypsin treatment using the mouse IgM monoclonal antibody 10E4 raised against HSPG (Seikagaku) (*31*). CHO-K1 cells (1.5×10^5) were treated with 0.01% trypsin in PBS (200 μL) at 37 °C for 10 min prior to two washings with PBS. The cells were treated with the above anti-HSPG antibody (1 mg/mL, 2 μL) in PBS (200 μL) at 4 °C for 30 min prior to two washings with PBS. The cells were then incubated with the Alexa488-labeled secondary antibody against the mouse IgM μ chain (Alexa Fluor 488 goat anti-mouse IgM μ chain) (Molecular Probes) (2 mg/mL, 4 μL) in PBS (200 μL) at 4 °C for 30 min prior to three washings with PBS and then subjected to a FACS analysis. As a control, the cells were detached from the dishes by a treatment with 2 mM EDTA at 37 °C for 5 min instead of trypsin, and similarly analyzed as already stated. The amount of cellular HSPG after the above trypsin treatment was less than 5% in the EDTA-treated cells (Supporting Information Figure S1). We also confirmed that the fluorescence from the cells treated at 4 °C was as low as the autofluorescence level (see Supporting Information Figure S2). These data suggest that the surface adsorbed peptides are effectively removed by the above trypsin treatment. Analysis of the cellular uptake by 293T and the syndecan-overexpressing cells was similarly conducted using DMEM containing 10% heat-inactivated fetal bovine serum as the medium. For examination of the effect of the macropinocytosis inhibitor 5-(*N*-ethyl-*N*-isopropyl)amiloride (EIPA) (*13*, *15*−*17*) on the cellular uptake of the peptides, the cells were incubated in serum-free Ham's F-12 medium for 4 h prior to the pretreatment with EIPA (100 μM) in the medium at 37 °C for 10 min. The cells were then treated with the peptide (final concentration, 10 μM) in the presence of 100 μM EIPA for 30 min and analyzed by FACS as already described.

Immunoblotting of Rac1 Activation. CHO-K1 cells were seeded in 60 mm culture dishes at a density of 8×10^5 cells/dish, cultured for 24 h, and serum-starved in serum-free medium for 24 h. The cells were then stimulated with the R8 and Tat peptides (without fluorescent moieties) (10 μM), and EGF (400 ng/mL) for 5 min at 37 °C and lysed for 5 min with the ice-cold cell lysis buffer (50 mM Tris-HCl, pH 7.4, 100 mM NaCl, 10 mM $MgCl_2$, 1% Triton X-100, 10% glycerol, 1 mM dithiothreitol, 1 mM phenylmethylsulfonyl fluoride, 1 μg/mL aprotinin, and 1 μg/mL leupeptin) containing 5 μg of the Cdc42/Rac interactive binding motif protein tagged with the glutathione S-transferase (GST-CRIB) (*32*). Cell lysates were then centrifuged for 5 min at 13400*g* at 4 °C, and the supernate was incubated with glutathione-Sepharose beads for 30 min at 4 °C. After the beads were washed with the cell lysis buffer, the bound proteins were eluted in the Laemmli sample buffer and separated by 12.5% sodium dodecyl sulfate−polyacrylamide gel electrophoresis (SDS−PAGE). The separated proteins were electrophoretically transferred onto a polyvinylidene difluoride membrane (Millipore). The membrane was blocked with 3% low fat milk in Tris-buffered saline and then incubated with a mouse monoclonal anti-Rac1 antibody (Transduction Laboratories) (1:1000 dilution). The Rac1 antibody was detected using a horseradish peroxidase-conjugated goat anti-mouse IgG antibody (Dako) and the ECL detection kit (Amersham Biosciences). A densitometry analysis was performed using NIH Image software, and the amount of GST-CRIB-bound Rac1 was normalized to the total amounts of Rac1 in the cell lysates. In the case of the HeLa cells, these cells were seeded in 60 mm culture dishes at a density of 6×10^5 cells/dish, cultured for 48 h, serum-starved in serum-free medium containing 1% bovine serum albumin (BSA) for 24 h, and then similarly treated with peptides.

Cell Ruffling Assay. The CHO cells were seeded into eight well Lab-Tek-II chamber slides (Nalge Nunc) at a density of 2.4×10^4 cells per well in Ham's F-12 containing 10% heat-inactivated calf serum for 48 h. The medium was replaced by fresh medium lacking serum, and the cells were incubated for 18 h. After two washings with PBS, the cells were treated with the R8 and Tat peptides (without fluorescent moieties) (10 μM) in Ham's F-12 for 2.5 min. The cells were then washed three times with PBS, fixed with 4% paraformaldehyde at room temperature for 10 min, treated with 0.5% Triton X-100 in PBS at room temperature for 2 min, and then washed again with PBS. The cellular F-actin was stained with phalloidin-TRITC as already described (*13*) and observed using a confocal scanning laser FV300 microscope (Olympus) equipped with a 40× objective.

RESULTS

Effects of Membrane-Associated Proteoglycans on the Cellular Uptake of Arginine-Rich Peptides. HSPG has been reported to be important in the internalization of the arginine-rich peptides (*20*−*24*) as well as the full length Tat protein (86 residues) (*25*−*28*). Various arginine-rich peptides, including the linear and the branched-chain oligoarginine peptides, also translocate through biological membranes. However, detailed studies on the effect of membrane-associated proteoglycans for their cellular uptake of these oligoarginine peptides have not been reported. We have now studied octaarginine (R8) as a representative oligoarginine peptide using the wild-type Chinese hamster ovary CHO cell line, CHO-K1, and two deficient mutants in the proteoglycan biosynthesis, D-677 and A-745. D-677 has a single mutation that affects both the *N*-acetylglucosaminyltransferase and glucuronosyltransferase activities necessary for the polymerization of the disaccharide chains of HSPG, and lacks HSPG. This mutant cell line produces approximately three times more chondroitin sulfate proteoglycan than the wild-type cells. The A-745 cell line lacks xylosyltransferase, an enzyme necessary for the initiation of the glycosaminoglycan (GAG) synthesis, and does not produce detectable levels of any proteoglycans (*26*). These cells were treated with Alexa488-labeled R8 and Tat peptides (Figure 1A) (10 μM each) at 37 °C for 30 min in Ham's F-12 containing 10% serum, washed, and trypsinized. The amount of the respective peptides taken up by these cells was then analyzed by FACS. The majority of the cell-surface adsorbed peptides are removed by trypsin treatment, and thus our data reflect the total cellular uptake of the peptides (the sum of endosome-trapped and cytosol-released peptides) (see Experimental Procedures). The amount of both peptides taken up by the cells was considerably lower in the A-745 cells (10−20%) compared with that in the CHO-K1 cells for these peptides (Figure 1B). In contrast to the uptake of the R8 peptide in the HSPG-deficient D-677 cells (76%), a significant decrease in the uptake was observed for the Tat peptide in the D-677 cells (34%), suggesting that the cellular uptake of the Tat peptides is highly dependent on HSPG. Similar observations

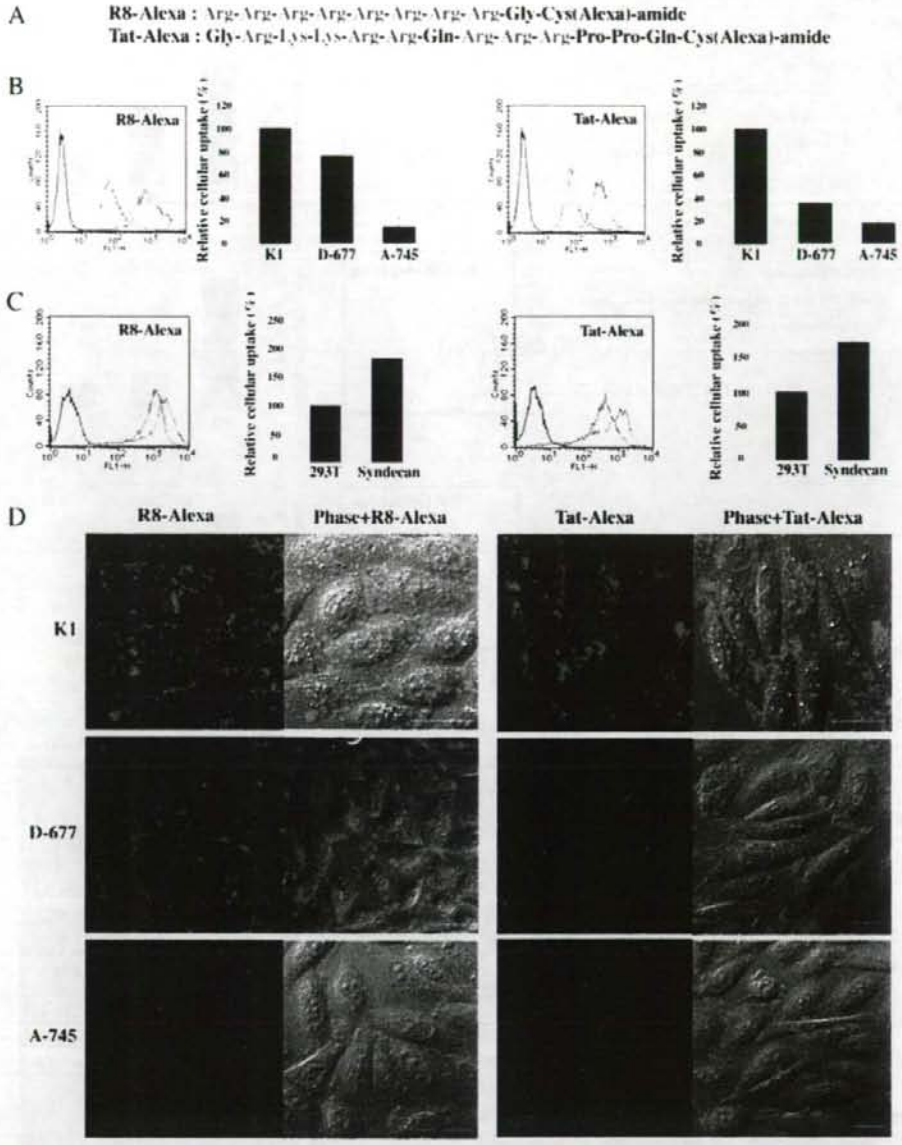

FIGURE 1: In contrast to the R8 peptide, the internalization of the Tat peptide is HSPG dependent. (A) Sequences of Alexa488-labeled R8 and Tat peptides. (B) FACS analysis of the proteoglycan-deficient cells treated with the Alexa488-labeled peptides (10 μM) at 37 °C for 30 min: green, CHO-K1 cells; red, A-745 cells; blue, D-677 cells. The amounts of the respective peptides taken up by these cells were normalized to the CHO-K1 cells as a standard. Error bars represent the mean ± standard deviation of 5 samples. (C) FACS analysis of the syndecan-2 overexpressing cells treated with Alexa488-labeled R8 and Tat peptides (10 μM) at 37 °C for 30 min: green, 293T cells; red, 293T-syndecan 2 cells. The results were normalized as the cellular uptake of the respective peptide by 293T cells as a standard. Error bars represent the mean ± standard deviation of 3 samples. (D) Confocal microscopy analysis of living CHO cells incubated with the Alexa488-labeled peptides (10 μM) at 37 °C for 30 min. Scale bar, 20 μm.

were previously observed in studies employing the fluorescein-labeled Tat peptide (*24*). On the other hand, the cellular uptake of the R8 peptide is not very highly dependent on HSPG as the Tat peptide. This suggests that the R8 peptide can be taken up by the cells by an alternative mechanism and/or via other proteoglycans.

Syndecan is one of the major classes of membrane-associated HSPGs. We next examined whether an increased cellular uptake of R8 and Tat is observed in 293T cells overexpressing syndecan-2 (*31*). The wild-type 293T cells and the mutant cell line overexpressing syndecan were treated with peptides (10 μM) for 30 min. Increases of 76% and 72% were observed for the uptake of the R8 and Tat peptides by the syndecan-2 overexpressing cells (Figure 1C), further supporting the importance of proteoglycan for the cellular uptake of the arginine-rich peptides.

Using confocal microscopy, we also studied the peptide internalization in a live control and mutant cells (Figure 1D). Since fixation was shown to cause significant artifacts on the cellular localization of peptides (*12*), and distribution of

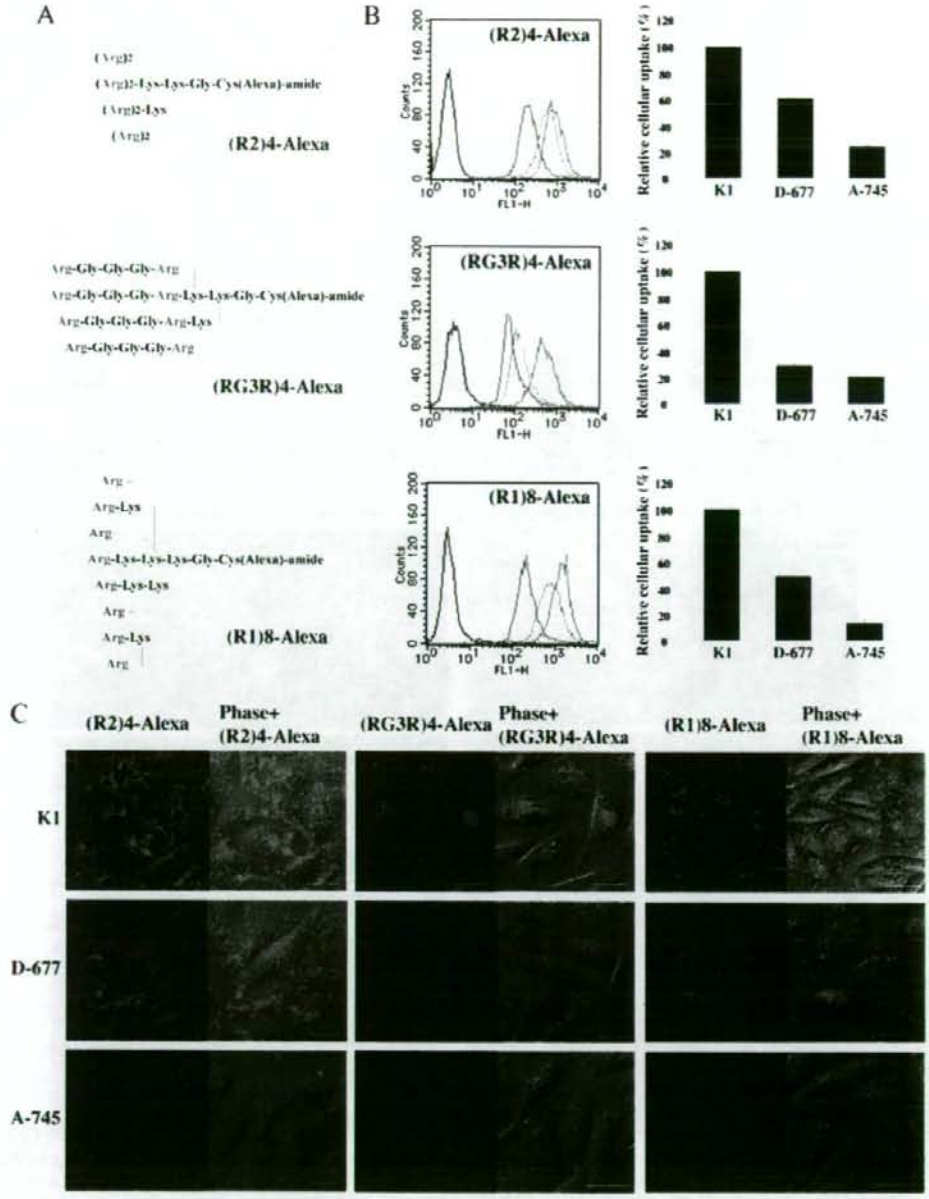

FIGURE 2: Comparison of branched-chain arginine-rich peptide uptake and their dependency on HSPG. (A) Structures of branched-chain arginine-rich peptides. (B) FACS analysis of the cells treated with (R2)4-Alexa, (RG3R)4-Alexa, and (R1)8-Alexa peptides (10 μM each) at 37 °C for 30 min: green, K1 cells; red, A-745 cells; blue, D-677 cells. The results were normalized as the cellular uptake of the respective peptides by CHO-K1 cells as a standard. Error bars represent the mean ± standard deviation of 3 samples. (C) Confocal microscopy analysis of living CHO cells incubated with branched-chain arginine-rich peptides (10 μM) at 37 °C for 30 min. Scale bar, 20 μm.

the fluorescently labeled peptides was then analyzed without fixing the cells. The punctate signals observed in the CHO-K1 cells suggest endosomal uptake of the peptides by the cells. On the other hand, a significant decreased amount of these punctate signals was observed in the A-745 cells. In the case of D-677 cells, punctate signals were predominantly observed only in the R8-treated cells. Significant increases in the amount of the punctate signals were also observed in the syndecan-2 overexpressing 293T cells compared with that in the wild-type 293T cells, supporting the results of the FACS analysis (data not shown). We concluded that proteoglycans mediate the endosomal peptide uptake that is peptide and proteoglycan type dependent.

We have previously reported that not only linear arginine-rich peptides but also the branched-chain peptides are internalized into cells, and that a cluster of arginines may be critical for their internalization (*7*). We also examined the role of the proteoglycans on the internalization of the branched-chain peptides. The Alexa488-labeled (R2)4, (RG3R)4, and (R1)8 peptides (Figure 2A) were selected as

examples of the branched-chain arginine-rich peptides. A significant decrease in the amount of the peptide taken up by the cells was observed in A-745 cells for all the peptides (Figure 2B). The cellular uptake by the A-745 cells of these peptides was less than 25% of that observed in CHO-K1 cells, confirming that proteoglycans play a crucial role in this process. The relative amount of the (RG3R)4 peptide taken up by the D-677 cells (28%) was considerably lower than that by the wild-type CHO-K1 cells and comparable to that observed in the A-745 cells (20%). On the other hand, the decrease in cellular uptake of the (R2)4 peptide by D-677 cells was much lower. A small but consistent decrease in the cellular uptake was also observed for the (R1)8 peptide compared to the other peptides. Therefore, the dependency on HSPG for cellular uptake of these peptides can be assigned (RG3R)4 > (R1)8 > (R2)4. These results suggest that the Tat and (RG3R)4 peptides can be internalized via similar mechanisms, whereas the uptake of (R1)8 and (R2)4 is internalized via a different mechanism, more akin to that observed for R8.

Similar results were observed in the confocal microscopic observations (Figure 2C). Punctate signals from the cells treated with these branched-chain peptides show endocytic cellular uptake of these peptides. The above results suggested that the cell-surface proteoglycans highly contribute to the cellular uptake of arginine-rich peptides and that the peptide structures may influence the interaction with HSPG.

Activation of Rac1 by Arginine-Rich Peptides. Macropinocytosis has been suggested in the cellular uptake of arginine peptides (*13*−*15*). We also reported that the organization of F-actin, which accompanies cellular uptake by macropinocytosis, is induced in HeLa cells by the arginine peptides (*13*). Rac has been reported to be involved in the F-actin organization, especially during the induction of lamellipodia (*33*, *34*). Rac is a member of the small molecular weight G protein Rho family and becomes active in its GTP-bound state (Rac-GTP) and inactive in its GDP-bound state (Rac-GDP). In the active state, Rac-GTP binds to various effector proteins by interacting with target motifs, such as the Cdc42/Rac interactive binding (CRIB) (*35*, *36*). We examined whether Rac1, a typical Rac protein, is activated by the arginine peptides. CHO-K1 cells were treated with the R8 or Tat peptide (10 μM) for 5 min. The cell lysates were then incubated with the CRIB motif protein which is tagged with GST (GST-CRIB) (*32*). Because the activated Rac1 (Rac1-GTP) can form a complex with GST-CRIB, this complex was isolated using a glutathione immobilized column, and the amount of the Rac1-GTP was analyzed by SDS−PAGE (Figure 3). The Rac1-GTP level increased 4.8- and 6.5-fold after treatment with the R8 and Tat peptides (10 μM), respectively. A 4.5-fold increase was obtained by treatment with the positive control, EGF (400 ng/mL). Therefore, the peptide treatment of the cells actually induces a significant activation of the Rac1 protein. Similarly, induction of Rac1 was also observed in HeLa cells by the treatment with these peptides; the Rac1-GTP level after treatment with the R8 and Tat peptides (10 μM) and EGF (400 ng/mL) was 3.1-, 6.5-, and 10.3-fold that of the control cells, respectively.

Effects of Proteoglycans on the Induction of Macropinocytosis and Actin Organization by Arginine-Rich Peptides. We next examined whether proteoglycans influence the

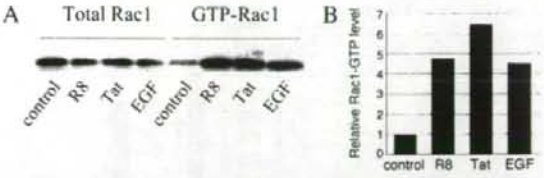

FIGURE 3: Activation of Rac1 by arginine-rich peptides. CHO-K1 cells were treated with the R8 peptide (10 μM), Tat peptide (10 μM), and EGF (400 ng/mL) for 5 min at 37 °C. The cell lysates were incubated with GST-CRIB, and the amounts of the GTP-bound Rac1 were determined by immunoblotting using a monoclonal anti-Rac1 antibody (A). Relative Rac1 activity was determined by the amount of GTP-bound Rac1 that was normalized to the amount of the total Rac1 in the cell lysates. The data were analyzed by NIH Image software, and the value from the control cells was arbitrarily set to 1. The average densitometric scan data of three samples are shown in B.

induction of macropinocytosis. We examined the effects of 5-(*N*-ethyl-*N*-isopropyl)amiloride (EIPA) on the cellular uptake of the arginine-rich peptides using CHO-K1, D-677, and A-745 cells (Figure 4). EIPA has been reported as a potent inhibitor of macropinocytosis (*16*, *17*). EIPA is known not to affect the clathrin-mediated endocytic uptake of transferrin, but it effectively inhibits the macropinocytic uptake of dextran stimulated by the epidermal growth factor (EGF) or adenovirus (*17*). Cells were pretreated with EIPA (100 μM) at 37 °C for 10 min in a serum-free medium, and then treated with the respective peptides (10 μM each) in the continued presence of 100 μM EIPA for 30 min. After trypsinization, the amount of the internalized peptide was quantified by FACS analysis. In this experiment, the fluorescent intensity from the cells treated with the respective peptides was analyzed without normalization to gain a better understanding of the quantitative differences in the total cellular uptake of the respective peptides.

A 56% decrease in the R8 peptide uptake by the wild-type CHO-K1 cells was observed in the presence of EIPA (Figure 4), suggesting that macropinocytosis contributes to the cellular uptake. In the case of the HSPG-deficient the D-677 cells, cellular uptake of the peptide in the absence and presence of EIPA was 78% and 17% of that in the CHO K-1 cells incubated with the peptide in the absence of EIPA. This suggests the possible involvement of macropinocytosis for the cellular uptake of the R8 peptide, even in the absence of HSPG. Our data suggest that HSPG may not be the only proteoglycan that contributes to the induction of macropinocytosis. The total cellular uptake of the R8 peptide by the proteoglycan-deficient A-745 cells was only 23% of that by the CHO K-1 cells incubated with the peptide in the absence of EIPA; there was only a minimal EIPA effect on the peptide uptake. This suggests that macropinocytosis may not be induced by the peptide in the absence of proteoglycans.

In the absence of EIPA, the cellular uptake of the Tat peptide is highly dependent on HSPG, and the quantities of the internalized peptide in the HSPG-deficient D-677 cells is almost as low as that in the proteoglycan-deficient A-745 cells (Figure 4). Macropinocytosis may also be important for the Tat uptake (Figure 4). Treatment of the wild-type CHO-K1 cells with the EIPA produced a 40% decrease in the cellular uptake of the Tat peptide. However, identical treatment of the A-745 cells revealed no significant differences in the Tat uptake in either the presence or absence of

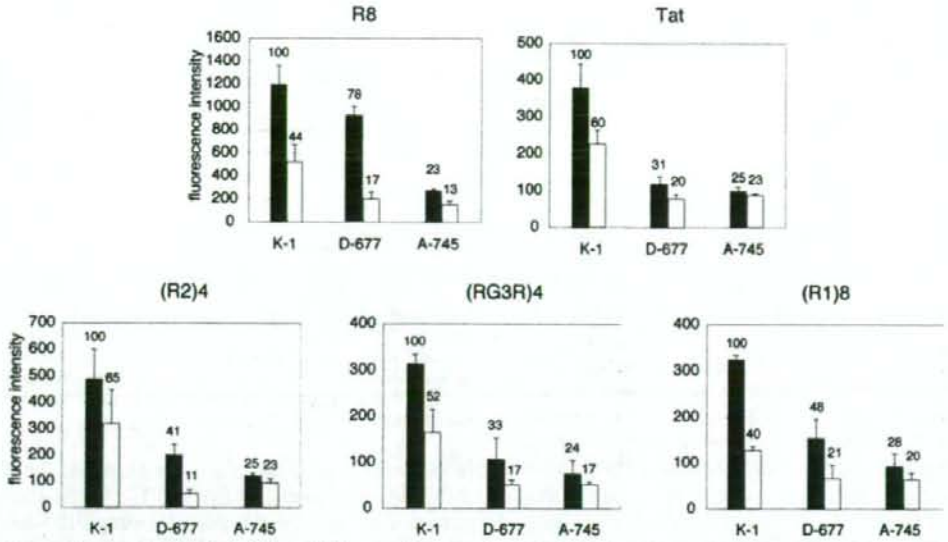

FIGURE 4: Effect of macropinocytosis inhibitor EIPA on cellular uptake of the arginine-rich peptides. The effect of the macropinocytosis inhibitor, 5-(*N*-ethyl-*N*-isopropyl)amiloride (EIPA), on the cellular uptake of the arginine-rich peptides was examined by FACS analysis. CHO cells (K1, D677, and A745) were initially pretreated with EIPA (100 μM) at 37 °C for 10 min in a serum-free medium. The cells were then incubated with the medium containing the Alexa488-labeled peptides (final concentration, 10 μM) in the presence of 100 μM EIPA for 30 min, prior to the trypsinization and FACS analysis. Fluorescence intensity (arbitrary unit) corresponds to the cellular uptake of the peptides in the absence (closed columns) and presence (open columns) of EIPA. Cellular uptake of the respective peptides under the given conditions is also shown as a percentage of the values observed in the untreated CHO-K1 cells. Error bars represent the mean ± standard deviation of 3−4 samples.

EIPA. Only minimal effects were observed by EIPA treatment in the D-677 cells. The lower uptake of the Tat peptide by the D-677 cells compared with lower effects on the R8 peptide uptake, together with the effect of EIPA on the D-677 cells, suggests that HSPG is important for the macropinocytic uptake of the Tat peptide.

We have demonstrated that the HSPG dependency for the peptide uptake of the branched-chain peptides is in the order (RG3R)4 > (R1)8 > (R2)4; the method of internalization of (RG3R)4 seems closer to that of Tat whereas (R2)4 is more comparable to R8 (Figure 2B). In addition, the R8 and (R2)4 are more efficiently internalized, especially by the CHO K-1 and D-677 cells, than the other peptides (Figure 4). The effect of EIPA on the cellular uptake of these branched peptides follows the same pattern. During the uptake of (R2)4 peptide by CHO-K1 cells, the EIPA treatment resulted in a 35% decrease in the cellular uptake of the peptide compared with cells incubated in the absence of this drug (Figure 4). An identical EIPA treatment of the D-677 cells inhibited the peptide uptake by 73% compared to the untreated cells; however, EIPA did not significantly inhibit the peptide uptake in the A-745 cells. Alternatively, though a significant decrease was observed for the uptake of the (RG3R)4 peptide by the CHO-K1 cells, the effect of EIPA on the uptake by the D-677 as well as the A-745 cells was not significant. The above results demonstrate that the inhibition effect of EIPA on the cellular uptake of the respective peptides is similar to the amount of their cellular uptake by these proteoglyan-deficient cells. This strongly suggests that the interaction of the peptides with proteoglycans should induce macropinocytosis. In addition, the peptide structures determine the specificity for proteoglycans in the macropinocytic uptake.

Macropinocytosis accompanies organization of the F-actin (*13*). We then examined whether the organization is observed in these proteoglycan-deficient CHO cells after incubations in R8 and Tat. The CHO-K1, D-677, and A-745 cells were treated with the respective peptides (10 μM), stained with the F-actin specific phalloidin-TRITC, and analyzed by confocal microscopy (Figure 5). Lamellipodia are thin, veil-like extensions at the edge of cells that contain a dynamic array of actin filaments. Although a very small amount of the lamellipodia-like structure was observed in the cells without the peptide treatment, a significant organization of F-actin, including lamellipodia-like structures (indicated by arrows in Figure 5), was observed in the CHO-K1 cells as early as 2.5 min after the treatment with these peptides. In contrast, neither a significant organization of the F-actin nor induction of the lamellipodia was observed for the A-745 cells. In the case of the D-677 cells, a significant induction of lamellipodia-like structures was observed by the R8 treatment, whereas a smaller degree of induction was observed in the Tat-treated cells (Figure 5). These results strongly suggest that cell-surface proteoglycans have an important biological role in the induction of macropinocytosis by the arginine-rich peptides. In addition, the lamellipodia formation in the HSPG-deficient D-677 cells supports the assumption that HSPG would not be a specific primary receptor for the induction of macropinocytosis by these peptides.

DISCUSSION

We have previously demonstrated that the cellular uptake of arginine-rich peptides, including the R8 and HIV-1 Tat peptides, is dependent on the cell-surface proteoglycans (*20*). We have also demonstrated that significant amounts of the

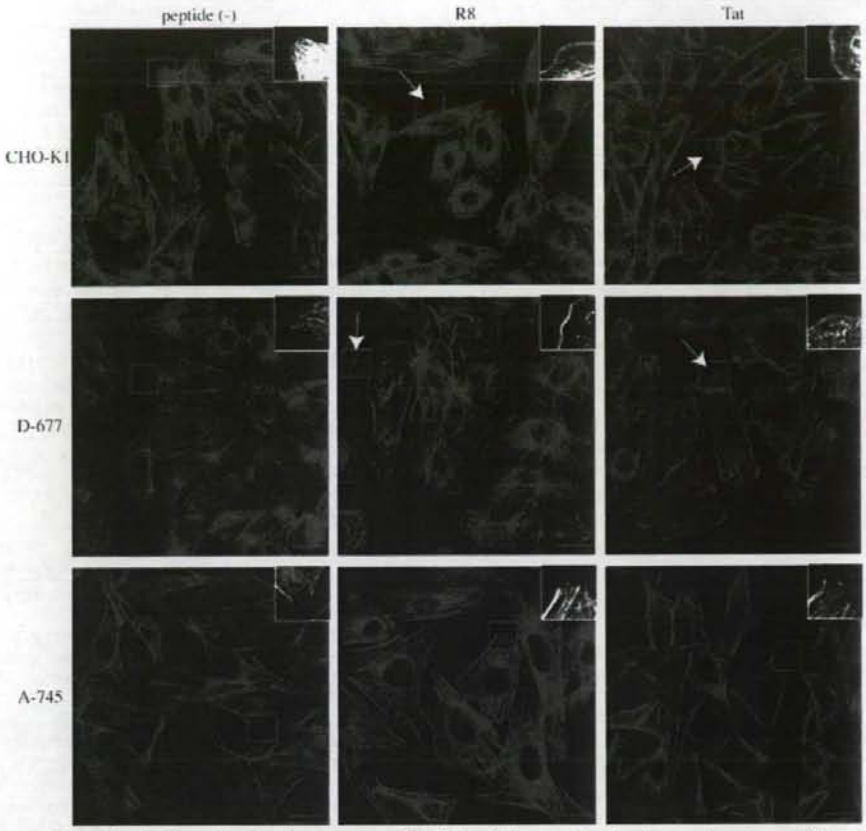

FIGURE 5: Absence of lamellipodia formation by the treatment of the R8 and Tat peptides in glycosaminoglycan deficient A745 cells. The CHO-K1, D-677, and A-475 cells were incubated in serum-free conditions for 18 h. After washing the cells twice with PBS, the cells were treated with the respective peptides (10 μM) in Ham's F-12 medium lacking serum for 2.5 min at 37 °C. After fixation of the cells using 4% paraformamide, the cells were stained with Phalloidin-TRITC. The arrows indicate the induced lamellipodia. Insets show images at ×2 magnification of boxed regions. Scale bar, 20 μm.

peptides are taken up by macropinocytosis (*13*). However, the relationship between the proteoglycans and the induction of macropinocytosis has not been elucidated. In this paper, we demonstrated that the cell-surface proteoglycans are required for the induction of macropinocytosis as demonstrated with the proteoglycan-deficient A-745 cells. A few minutes after treatment of the cells with arginine-rich peptides, activation of the Rac protein and organization of the actin were observed. This suggests that a quick cellular response is induced by these peptides.

HSPG has been suggested as the cellular receptor of the Tat peptide as well as for the full-length Tat protein (86 residues) (*20*−*28*). However, we have demonstrated here that the structures of the arginine-rich peptides determine this dependency. The branched-chain (RG3R)4 peptide also shows a high specificity for HSPG. Although proteoglycans play a crucial role in the cellular uptake of the R8, (R2)4, and (R1)8 peptides, uptake of these peptides appears less dependent on HSPG. The precise reason to explain these differences in HSPG specificity is not clear at this stage, but one possible reason could be the differences in the charge density. The former group contains other amino acids intervening between the arginine residues, whereas the latter consists of only arginines. It has been reported that the sulfuric acid content of HSPG is higher than other membrane-associated proteoglycans, such as chondroitin sulfate (*37*). The Tat and (RG3R)4 peptides, which have a smaller charge density than R8, can interact with HSPG, but may fail to interact with proteoglycans having a smaller negative charge density. The peptides in the latter group have a higher positive charge density and thus may be able to interact with other proteoglycans than HSPG to initiate cellular uptake. An alternative explanation, but maybe less plausible, is that the Tat and (RG3R)4 have conformations that promote the interaction with HSPG. A further study is necessary to clarify this mechanism. However, the above results strongly suggest that HSPG is not the only receptor to induce macropinocytic uptake of R8 and other oligoarginine peptides. Lamellipodia formation and induction of macropinocytosis in D-677 cells by the R8 peptide treatment even in the absence of HSPG further support this idea of their receptors.

In this study, we have shown that the Rac protein, which induces membrane ruffles that are enriched with actin filaments around the boundary of cells, was actually activated as early as 5 min after the treatment of the cells with the Tat and R8 peptides. This correlates with the lamellipodia formation observed 2.5 min after the peptide treatment. These results indicate that certain rapid cellular signals are transmitted by the interaction of these peptides with the cells to induce actin organization and macropinocytosis.

How can the peptide signals be transmitted to Rac to induce the eventual actin organization and macropinocytosis? It is known that an interaction with HSPG is critical for activation of certain receptors by growth factors, such as the fibroblast growth factor (FGF) (*38*). One possible idea is that the arginine-rich peptides may activate the receptors of bioactive proteins, including growth factors such as FGF, in collaboration with proteoglycans. These peptides likely do not have a specificity for these receptors, since there are no consensus sequences among the arginine-rich peptides except that they have clusters of arginines or guanidinium moieties in their molecules. It has been suggested that the full-length Tat protein (86 residues) could activate a vascular endothelial growth factor (VEGF) receptor (*39*), although the Tat peptide is not a high-affinity ligand for the receptor (*40*). However, there remains the possibility that these arginine peptides activate a receptor in the concentration ranges of nonspecific interactions. A 10 μM R8 peptide and 10 nM EGF induce a similar actin organization, in which there is a 3-order of concentration difference (*13*). In addition, there is a report on the induction of actin organization by the full length Tat protein at the concentration of ~5 nM (*41*). However, the Tat and R8 peptides do not influence actin at this concentration (data not shown). It seems likely that domains other than the basic domain in the Tat protein would contribute to the specificity or give a high binding affinity. This also suggests that the biological effects induced by the Tat and other arginine-rich peptides are not necessarily identical to those of the full-length Tat protein.

As an alternative possibility, arginine-rich peptides may compete with the binding of the bioactive proteins by proteoglycans. This competition may lead to a release of the matrix-trapped proteins that interact with their specific receptors. It has also been proposed that the interaction of extracellular ligands with syndecan leads the multimerization of syndecan to induce actin polymerization (*42*), and arginine-rich peptides might have a similar effect on the signal transduction via syndecan multimerization.

Interestingly, lamellipodia formation was also observed in the Tat-treated D-677 cells whose cellular uptake of these peptides is considerably lower than that observed in the CHO-K1 cells. Further studies are necessary to determine why this is the case. We can, however, hypothesize that the cellular uptake of the arginine-rich peptides would be determined by the balance between the extent of their ability to induce macropinocytosis and their affinity to the plasma membrane. Assuming that the Tat peptide can still bind proteoglycans other than HSPG even with a lower affinity, the higher ability of Tat, compared to R8, to activate Rac1 as shown in this report may yield lamellipodia formation to some extent. However, this may not be reflected in the cellular uptake level due to its lower affinity to D-677 cells. A similar idea would be applicable to analyze the cellular uptake by the wild-type CHO-K1 cells. The Tat peptide can activate the Rac1 more effectively than the R8 peptide whereas the more positively charged R8 peptide would yield a significantly higher cellular uptake than the Tat peptide. Therefore, not only the ability to induce macropinocytosis but also their affinity to the plasma membrane should be taken into account in order to consider the efficacy of the peptides for cellular uptake.

In conclusion, this report highlights the possibility that the binding of arginine-rich peptides with the cell surface proteoglycans activates intracellular signals that lead to the actin organization and macropinocytosis. This binding step is required for the induction of the macropinocytic uptake of the peptides. EIPA is an inhibitor of the Na^+/H^+ antiporter required for macropinocytosis, and further work is necessary for the effect of the disruption of ionic equilibrium operated by EIPA on the internalization of the peptides. However, the results obtained in this study provide novel insights into the internalization mechanisms of the arginine-rich peptides and are useful for the design and development of more sophisticated delivery systems using peptide vectors.

SUPPORTING INFORMATION AVAILABLE

HPLC retention times for the synthetic peptides and FACS analysis of the cellular fluorescence/HSPG after trypsin treatment. This material is available free of charge via the Internet at http://pubs.acs.org.

REFERENCES

1. Fawell, S., Seery, J., Daikh, Y., Moore, C., Chen, L. L., Pepinsky, B., and Barsoum, J. (1994) Tat-mediated delivery of heterologous proteins into cells, *Proc. Natl. Acad. Sci. U.S.A. 91*, 664−668.
2. Vives, E., Brodin, P., and Lebleu, B. (1997) A truncated HIV-1 Tat protein basic domain rapidly translocates through the plasma membrane and accumulates in the cell nucleus, *J. Biol. Chem. 272*, 16010−16017.
3. Wadia, J. S., and Dowdy, S. F. (2005) Transmembrane delivery of protein and peptide drugs by TAT-mediated transduction in the treatment of cancer, *Adv. Drug Delivery Rev. 57*, 579−596.
4. Derossi, D., Joliot, A. H., Chassaing, G., and Prochiantz, A. (1994) The third helix of the Antennapedia homeodomain translocates through biological membranes, *J. Biol. Chem. 269*, 10444−10450.
5. Joliot, A., and Prochiantz, A. (2004) Transduction peptides: from technology to physiology, *Nat. Cell Biol. 6*, 189−196.
6. Futaki, S., Suzuki, T., Ohashi, W., Yagami, T., Tanaka, S., Ueda, K., and Sugiura, Y. (2001) Arginine-rich peptides. An abundant source of membrane-permeable peptides having potential as carriers for intracellular protein delivery, *J. Biol. Chem. 276*, 5836−5840.
7. Futaki, S., Nakase, I., Suzuki, T., Youjun, Z., and Sugiura, Y. (2002) Translocation of branched-chain arginine peptides through cell membranes: flexibility in the spatial disposition of positive charges in membrane-permeable peptides, *Biochemistry 41*, 7925−7930.
8. Wender, P. A., Mitchell, D. J., Pattabiraman, K., Pelkey, E. T., Steinman, L., and Rothbard, J. B. (2000) The design, synthesis, and evaluation of molecules that enable or enhance cellular uptake: peptoid molecular transporters, *Proc. Natl. Acad. Sci. U.S.A. 97*, 13003−13008.
9. Rothbard, J. B., Kreider, E., VanDeusen, C. L., Wright, L., Wylie, B. L., and Wender, P. A. (2002) Arginine-rich molecular transporters for drug delivery: role of backbone spacing in cellular uptake, *J. Med. Chem. 45*, 3612−3618.
10. Umezawa, N., Gelman, M. A., Haigis, M. C., Raines, R. T., and Gellman, S. H. (2002) Translocation of a beta-peptide across cell membranes, *J. Am. Chem. Soc. 124*, 368−369.
11. Futaki, S. (2005) Membrane-permeable arginine-rich peptides and the translocation mechanisms, *Adv. Drug Delivery Rev. 57*, 547−558.
12. Richard, J. P., Melikov, K., Vives, E., Ramos, C., Verbeure, B., Gait, M. J., Chernomordik, L. V., and Lebleu, B. (2003) Cell-penetrating peptides. A reevaluation of the mechanism of cellular uptake, *J. Biol. Chem. 278*, 585−590.
13. Nakase, I., Niwa, M., Takeuchi, T., Sonomura, K., Kawabata, N., Koike, Y., Takehashi, M., Tanaka, S., Ueda, K., Simpson, J. C., Jones, A. T., Sugiura, Y., and Futaki, S. (2004) Cellular uptake of arginine-rich peptides: roles for macropinocytosis and actin rearrangement, *Mol. Ther. 10*, 1011−1022.

14. Wadia, J. S., Stan, R. V., and Dowdy, S. F. (2004) Transducible TAT-HA fusogenic peptide enhances escape of TAT-fusion proteins after lipid raft macropinocytosis, *Nat. Med. 10*, 310−315.
15. Kaplan, I. M., Wadia, J. S., and Dowdy, S. F. (2005) Cationic TAT peptide transduction domain enters cells by macropinocytosis, *J. Controlled Release 102*, 247−253.
16. Swanson, J. A., and Watts, C. (1995) Macropinocytosis. *Trends Cell Biol. 5*, 424−428.
17. Meier, O., Boucke, K., Hammer, S. V., Keller, S., Stidwill, R. P., Hemmi, S., and Greber, U. F. (2002) Adenovirus triggers macropinocytosis and endosomal leakage together with its clathrin-mediated uptake, *J. Cell Biol. 158*, 1119−1131.
18. Meier, O., and Greber, U. F. (2003) Adenovirus endocytosis, *J. Gene Med. 5*, 451−462.
19. Conner, S. D., and Schmid, S. L. (2003) Regulated portals of entry into the cell, *Nature 422*, 37−44.
20. Suzuki, T., Futaki, S., Niwa, M., Tanaka, S., Ueda, K., and Sugiura, Y. (2002) Possible existence of common internalization mechanisms among arginine-rich peptides, *J. Biol. Chem. 277*, 2437−2443.
21. Console, S., Marty, C., García-Echeverría, C., Schwendener, R., and Ballmer-Hofer, K. (2003) Antennapedia and HIV transactivator of transcription (TAT) "protein transduction domains" promote endocytosis of high molecular weight cargo upon binding to cell surface glycosaminoglycans, *J. Biol. Chem. 278*, 35109−35114.
22. Ziegler, A., and Seelig, J. (2004) Interaction of the protein transduction domain of HIV-1 TAT with heparan sulfate: binding mechanism and thermodynamic parameters, *Biophys. J. 86*, 254−263.
23. Fuchs, S. M., and Raines, R. T. (2004) Pathway for polyarginine entry into mammalian cells, *Biochemistry 43*, 2438−2444.
24. Richard, J. P., Melikov, K., Brooks, H., Prevot, P., Lebleu, B., and Chernomordik, L. V. (2005) Cellular uptake of unconjugated TAT peptide involves clathrin-dependent endocytosis and heparan sulfate receptors, *J. Biol. Chem. 280*, 15300−15306.
25. Chang, H. C., Samaniego, F., Nair, B. C., Buonaguro, L., and Ensoli, B. (1997) HIV-1 Tat protein exits from cells via a leaderless secretory pathway and binds to extracellular matrix-associated heparan sulfate proteoglycans through its basic region, *AIDS 11*, 1421−1431.
26. Tyagi, M., Rusnati, M., Presta, M., and Giacca, M. (2001) Internalization of HIV-1 tat requires cell surface heparan sulfate proteoglycans, *J. Biol. Chem. 276*, 3254−3261.
27. Rusnati, M., Coltrini, D., Oreste, P., Zoppetti, G., Albini, A., Noonan, D., d'Adda di Fagagna, F., Giacca, M., and Presta, M. (1997) Interaction of HIV-1 Tat protein with heparin. Role of the backbone structure, sulfation, and size, *J. Biol. Chem. 272*, 11313−11320.
28. Liu, Y., Jones, M., Hingtgen, C. M., Bu, G., Laribee, N., Tanzi, R. E., Moir, R. D., Nath, A., and He, J. J. (2000) Uptake of HIV-1 tat protein mediated by low-density lipoprotein receptor-related protein disrupts the neuronal metabolic balance of the receptor ligands, *Nat. Med. 6*, 1380−1387.
29. Sanderson, R. D., Yang, Y., Suva, L. J., and Kelly, T. (2004) Heparan sulfate proteoglycans and heparanase—partners in osteolytic tumor growth and metastasis, *Matrix Biol. 23*, 341−352.
30. Sasisekharan, R., Shriver, Z., Venkataraman, G., and Narayanasami, U. (2002) Roles of heparan-sulphate glycosaminoglycans in cancer, *Nat. Rev. Cancer 2*, 521−528.
31. Utani, A., Nomizu, M., Matsuura, H., Kato, K., Kobayashi, T., Takeda, U., Aota, S., Nielsen, P. K., and Shinkai, H. (2001) A unique sequence of the laminin alpha 3 G domain binds to heparin and promotes cell adhesion through syndecan-2 and -4, *J. Biol. Chem. 276*, 28779−28788.
32. Katoh, H., and Negishi, M. (2003) RhoG activates Rac1 by direct interaction with the Dock180-binding protein Elmo, *Nature 424*, 461−464.
33. Schlunck, G., Damke, H., Kiosses, W. B., Rusk, N., Symons, M. H., Waterman-Storer, C. M., Schmid, S. L., and Schwartz, M. A. (2004) Modulation of Rac localization and function by dynamin, *Mol. Biol. Cell 15*, 256−267.
34. Marcoux, N., and Vuori, K. (2003) EGF receptor mediates adhesion-dependent activation of the Rac GTPase: a role for phosphatidylinositol 3-kinase and Vav2, *Oncogene 22*, 6100−6106.
35. Noda, Y., Takeya, R., Ohno, S., Naito, S., Ito, T., and Sumimoto, H. (2001) Human homologues of the Caenorhabditis elegans cell polarity protein PAR6 as an adaptor that links the small GTPases Rac and Cdc42 to atypical protein kinase C, *Genes Cells 6*, 107−119.
36. Burbelo, P. D., Drechsel, D., and Hall, A. (1995) A conserved binding motif defines numerous candidate target proteins for both Cdc42 and Rac GTPases, *J. Biol. Chem. 270*, 29071−29074.
37. Ueno, M., Yamada, S., Zako, M., Bernfield, M., and Sugahara, K. (2001) Structural characterization of heparan sulfate and chondroitin sulfate of syndecan-1 purified from normal murine mammary gland epithelial cells. Common phosphorylation of xylose and differential sulfation of galactose in the protein linkage region tetrasaccharide sequence, *J. Biol. Chem. 276*, 29134−29140.
38. Pellegrini, L. (2001) Role of heparan sulfate in fibroblast growth factor signalling: a structural view, *Curr. Opin. Struct. Biol. 11*, 629−634.
39. Mitola, S., Sozzani, S., Luini, W., Primo, L., Borsatti, A., Weich, H., and Bussolino, F. (1997) Tat-human immunodeficiency virus-1 induces human monocyte chemotaxis by activation of vascular endothelial growth factor receptor-1, *Blood 90*, 1365−1372.
40. Rubio Demirovic, A., Canadi, J., Weiglhofer, W., Scheidegger, P., Jaussi, R., and Kurt, B. H. (2003) HIV TAT basic peptide is not a high-affinity ligand for VEGF receptor 2, *Biol. Chem. 384*, 1435−1441.
41. Wu, R. F., Gu, Y., Xu, Y. C., Mitola, S., Bussolino, F., and Terada, L. S. (2004) Human immunodeficiency virus type 1 Tat regulates endothelial cell actin cytoskeletal dynamics through PAK1 activation and oxidant production, *J. Virol. 78*, 779−789.
42. McQuade, K. J., and Rapraeger, A. C. (2003) Syndecan-1 transmembrane and extracellular domains have unique and distinct roles in cell spreading, *J. Biol. Chem. 278*, 46607−46615.

BI0612824

BJ www.biochemj.org

BJ Cell

Biochem. J. (2007) **403**, 335–342 (Printed in Great Britain) doi:10.1042/BJ20061808

Temperature-, concentration- and cholesterol-dependent translocation of L- and D-octa-arginine across the plasma and nuclear membrane of CD34+ leukaemia cells

Marjan M. FRETZ*†, Neal A. PENNING*, Saly AL-TAEI*, Shiroh FUTAKI‡§, Toshihide TAKEUCHI‡, Ikuhiko NAKASE‡, Gert STORM† and Arwyn T. JONES*[1]

*Welsh School of Pharmacy, Cardiff University, Cardiff CF10 3XF, Wales, U.K., †Department of Pharmaceutics, Utrecht Institute for Pharmaceutical Sciences, Utrecht University, PO Box 80082, 3508 TB Utrecht, The Netherlands, ‡Institute for Chemical Research, Kyoto University, Uji, Kyoto 611-0011, Japan, and §PRESTO, Japan Science and Technology Agency (JST), Kawaguchi, Saitama 332-0012, Japan

Delineating the mechanisms by which cell-penetrating peptides, such as HIV-Tat peptide, oligoarginines and penetratin, gain access to cells has recently received intense scrutiny. Heightened interest in these entities stems from their ability to enhance cellular delivery of associated macromolecules, such as genes and proteins, suggesting that they may have widespread applications as drug-delivery vectors. Proposed uptake mechanisms include energy-independent plasma membrane translocation and energy-dependent vesicular uptake and internalization through endocytic pathways. In the present study, we investigated the effects of temperature, peptide concentration and plasma membrane cholesterol levels on the uptake of a model cell-penetrating peptide, L-octa-arginine (L-R8) and its D-enantiomer (D-R8) in CD34+ leukaemia cells. We found that, at 4–12 °C, L-R8 uniformly labels the cytoplasm and nucleus, but in cells incubated with D-R8 there is additional labelling of the nucleolus which is still prominent at 30 °C incubations. At temperatures between 12 and 30 °C, the peptides are also localized to endocytic vesicles which consequently appear as the only labelled structures in cells incubated at 37 °C. Small increases in the extracellular peptide concentration in 37 °C incubations result in a dramatic increase in the fraction of the peptide that is localized to the cytosol and promoted the binding of D-R8 to the nucleolus. Enhanced labelling of the cytosol, nucleus and nucleolus was also achieved by extraction of plasma membrane cholesterol with methyl-β-cyclodextrin. The data argue for two, temperature-dependent, uptake mechanism for these peptides and for the existence of a threshold concentration for endocytic uptake that when exceeded promotes direct translocation across the plasma membrane.

Key words: cell-penetrating peptide, endocytosis, fluorescence microscopy, KG1a cell line, leukaemia, octa-arginine.

INTRODUCTION

The scientific literature describes an ever-increasing library of peptides that mediate the lysis of biological membranes or have capacities to translocate through these structures in the absence of increasing porosity to other molecules. An example of the former is mellitin, but recently more attention has been focused on CPPs (cell-penetrating peptides), also called protein transduction domains, such as the Tat peptide from the HIV-Tat protein and penetratin from the *Drosophila melanogaster* homeobox protein Antennapedia [1]. A particular interest in these CPPs derives from their abilities *in vitro* and *in vivo* to overcome cellular barriers, such as the plasma membrane, and deliver therapeutic macromolecular cargo, including genes and proteins, into cells [2–5].

A prerequisite to efficient utilization of these peptides as delivery vectors is an enhanced understanding of: (i) their interaction with cell-surface components, such as proteins, carbohydrates and lipids; (ii) their mechanism of uptake, such as endocytosis and direct translocation; and (iii) their intracellular fate, such as delivery to lysosomes, dynamics in the cytosol and delivery to the nucleus. Since the discovery that a number of CPP effects are due to fixation artefacts [6,7], the concept that cellular entry was via direct plasma membrane translocation has been somewhat superseded by models showing that entry is via some form of endocytic route, and that translocation occurs across membranes of the endo/lysosomal system or even the endoplasmic reticulum [7–11]. These studies mostly relate to microscopic and flow-cytometric analysis of the peptides as fluorescent conjugates; their attachment to larger cargo will undoubtedly affect their interactions with cells and their translocation capacities [12,13].

Studies from our laboratories and others, using oligoarginine (R7–R9) and HIV-Tat peptides, have shown, however, that, despite the use of stringent methods to remove plasma-membrane-associated peptides with trypsin and heparin, a significant fraction enters cells and nucleus at 4 °C [11,12,14,15]. Uptake of fluorescent HIV-Tat and R8 (octa-arginine) peptides in the non-adherent leukaemic KG1a cell line was not inhibited by placing the cells on ice, but the labelling was diffusely localized throughout the cells compared with only vesicular labelling at 37 °C [11]. Similar observations have been demonstrated in a number of adherent cell lines [12,14,15]. Other studies in HUVECs (human umbilical vein endothelial cells) and macrophages show that 4 °C incubations inhibited uptake by ~75 % compared with incubations performed at 37 °C [10], and claims also exist for no uptake at 4 °C [9]. Although there is disparity over the extent of cellular association at 4 °C, there is general uniformity with respect to the fact that a significant fraction enters cells in the absence of endocytic mechanisms. Recent data also suggest that R8 was able to enhance delivery of liposomes at both 37 and 4 °C [16].

Model membrane systems have also been utilized to investigate the translocation capacities of these peptides, and, as expected, this process is dependent on the peptide sequence and the lipid

Abbreviations used: CM, complete RPMI 1640 medium; CPP, cell-penetrating peptide; MβCD, methyl-β-cyclodextrin; MTT, 3-(4,5-dimethylthiazol-2-yl)-2,5-diphenyl-2*H*-tetrazolium bromide; PI, propidium iodide; R8, octa-arginine; SFM, serum-free RPMI 1640 medium; Tf, transferrin.

[1] To whom correspondence should be addressed (email jonesat@cardiff.ac.uk).

© The Authors Journal compilation © 2007 Biochemical Society

Biochemical Journal

composition of the membranes [17–21]. These studies have allowed for proposals for the mechanism by which the peptides interact with and traverse membrane systems, and favoured models suggest they are driven via a potential difference following membrane destabilization, that they induce the formation of inverted micelles or that they themselves mediate pore formation.

To investigate further the effects of temperature on cellular peptide uptake, we have performed quantitative and qualitative analysis with the model CPP L-R8–Alexa Fluor® 488 and its D-enantiomer in a leukaemic cell line. We found that peptide localization is sensitive to cholesterol sequestration, peptide concentration and the incubation temperature, such that a reduction in endocytosis at low temperatures is paralleled by an increase in peptide translocation through the plasma membrane.

EXPERIMENTAL

Materials

Alexa Fluor® 488–C_5–maleimide and Alexa Fluor 488®–Tf (transferrin) were from Invitrogen. DRAQ5 dye was a gift from Biostatus. *N*-Acetylcysteine and MβCD (methyl-β-cyclodextrin) were purchased from Sigma.

Peptide synthesis

The two peptides used in the present study were generated as previously described by Fmoc (fluoren-9-ylmethoxycarbonyl) solid-phase synthesis and labelled at the C-terminal cysteine using Alexa Fluor® 488–C_5–maleimide sodium salt as fluorescent dye [11]. Purification and characterization were achieved by HPLC and MALDI–TOF (matrix-assisted laser-desorption ionization–time-of-flight) MS respectively. The final peptide products were L-R8–Alexa Fluor® 488 containing naturally abundant L-arginine [NH_2-(L-Arg)$_8$-Gly-Cys-(Alexa Fluor® 488)-amide] or D-R8–Alexa Fluor® 488 [NH_2-(D-Arg)$_8$-Gly-Cys-(Alexa Fluor® 488)-amide].

Cell culture

The haemopoietic cell line KG1a was maintained at confluency of (0.5–2) $\times$ 10^6 cells/ml in RPMI 1640 medium supplemented with 10% (v/v) fetal calf serum, 100 IU/ml penicillin and 100 μg/ml streptomycin at 37 °C with 5% CO_2 in humidified air. All cell culture reagents were obtained from Invitrogen.

Fluorescence microscopy

KG1a cells (0.5 $\times$ 10^6) were washed once with CM (complete RPMI 1640 medium) and equilibrated for 15 min in CM set at 4 (ice), 12, 19, 30 and 37 °C. The medium was then replaced with 200 μl of fresh equilibrated CM containing 2–10 μM L- or D-R8–Alexa Fluor® 488 or 100 nM Alexa Fluor® 488–Tf and incubated at these temperatures for 1 h. The cells were washed twice with ice-cold PBS and once with SFM (serum-free RPMI 1640 medium) without Phenol Red, serum or antibiotics (imaging medium), and resuspended in approx. 20 μl of imaging medium. In some experiments, 10 μM DRAQ5 dye was used to label the nucleus, and this was added at room temperature (20 °C) for 3 min before the last washing step.

Finally, 2 μl of the cell suspension was transferred to a well of a ten-well multispot microscope slide (Hendley) that was then layered with a coverslip. Live cells were then immediately analysed by fluorescence microscopy. Wide-field fluorescent images were obtained on a Leica DMIRB inverted fluorescence microscope equipped with a 63$\times$ oil-immersion objective and QImaging Retiga 1300 camera. The acquired images were processed with Improvision Openlab 5.0.2 software. Confocal microscopy was performed using a Leica TCS-SP2 RS confocal laser-scanning microscope equipped with an Ar and HeNe laser and a 63$\times$ oil-immersion objective. Leica LCS Lite software was used to merge and stack individual confocal sections through the *z*-axis to generate maximum projection images. Supplementary movies (see http://www.BiochemJ.org/bj/403/bj4030335add.htm) were generated from the *z*-stacks using NIH (National Institutes of Health) ImageJ 1.36b software.

In one designated experiment, cells were incubated with 2 μM L-R8–Alexa Fluor® 488 for 1 h and, following washing, were fixed in 3% (w/v) paraformaldehyde for 15 min before further washes and analysis by fluorescence microscopy.

Flow cytometry

KG1a cells (0.5 $\times$ 10^6) were equilibrated and incubated for 1 h with 2 μM L- or D-R8–Alexa Fluor® 488 at different temperatures as described above. Alternatively, cells were washed in ice-cold CM and incubated with 0.25–5 μM L- or D-R8–Alexa Fluor® 488 for 1 h at 4 °C. The cells were washed three times with ice-cold PBS, resuspended in 200 μl of PBS and Alexa Fluor® 488 fluorescence was measured using a Becton Dickinson FACScalibur analyser. In some experiments, following peptide incubation, the cells were washed once with PBS, incubated with 0.25 mg/ml trypsin solution for 5 min at 37 °C, washed once with ice-cold PBS and finally twice with PBS containing 14 μg/ml heparin. Live cells were gated on forward scatter and side scatter, and 10000 viable cells were analysed.

Analysis of binding and uptake of activated and inactivated Alexa Fluor® 488–C_5–maleimide

Unconjugated (activated) Alexa Fluor® 488–C_5–maleimide was dissolved in methanol to a concentration of 1.78 mM. For inactivation, 375 μl of the solution was incubated at room temperature for 4 h with a 4-fold molar excess of *N*-acetylcysteine (10 mg/ml in PBS). The solution was then stored at −20 °C until use. For cell studies, KG1a cells (0.5 $\times$ 10^6) were equilibrated on ice or at 37 °C, washed and incubated further on ice or at 37 °C in CM containing 2 μM activated or inactivated dye. Finally, the cells were washed twice with imaging medium and analysed, as described, by fluorescence microscopy.

Binding and uptake of peptides and Tf by MβCD-treated cells

MβCD was dissolved in PBS to 76 mM and diluted to 5 mM in SFM. KG1a cells (0.5 $\times$ 10^6) were washed once with SFM, resuspended in 200 μl of SFM containing 5 mM MβCD and incubated under tissue-culture conditions for 30 min. Control cells were treated as above, but in the absence of MβCD. The cells were then washed with SFM and incubated for 1 h at 37 °C with 2 μM L- or D-R8–Alexa Fluor® 488 or 100 nM Alexa Fluor® 488–Tf in SFM. The cells were washed twice with SFM, resuspended in imaging medium and analysed by fluorescence microscopy.

Cell viability studies

KG1a cells (4 $\times$ 10^4 cells/well in a total volume of 200 μl) were seeded in 96-well plates and incubated with 0–50 μM L- or D-R8–Alexa Fluor® 488 for 24 h under tissue-culture conditions. Cell viability was then assessed using MTT [3-(4,5-dimethylthiazol-2-yl)-2,5-diphenyl-2*H*-tetrazolium bromide] assays [22]. Briefly,

© The Authors Journal compilation © 2007 Biochemical Society

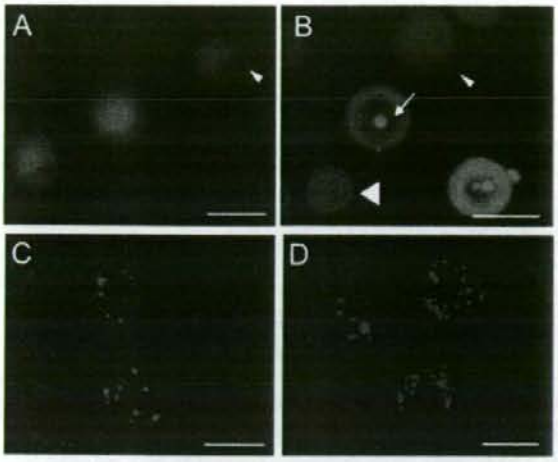

Figure 1 Cellular distribution of L- and D-R8–Alexa Fluor® 488 in KG1a cells at 4 and 37 °C

KG1a cells were incubated for 1 h with 2 μM L- (**A**, **C**) or D-R8–Alexa Fluor® 488 (**B**, **D**) at either 4 (**A**, **B**) or 37 °C (**C**, **D**), before analysis by confocal microscopy. Shown are maximum projections of 35 *z*-stacks (~500 nm and 2–4 s/section) for each condition. (**A**) and (**B**) were also labelled with DRAQ5 dye as described in the Experimental section. Arrows in (**B**) indicate peptide labelling of nucleolus, the small arrowhead shows a cell showing low peptide labelling, and the large arrowhead shows a cell with undetectable levels of peptide fluorescence. Scale bars, 10 μm. Supplementary Movies 1–4 at http://www.BiochemJ.org/bj/403/bj4030335add.htm display the contribution of each individual stack to the overall fluorescence.

20 μl of MTT, 5.5 mg/ml in SFM, was added directly to each well, giving a final concentration of 0.5 mg/ml. The cells were then incubated for 4 h under tissue-culture conditions. The plates were centrifuged at 1000 *g* for 5 min before removing the supernatant and then adding 100 μl of DMSO. The samples were finally incubated at 37 °C for 30 min before quantifying the absorbance at 550 nm.

RESULTS AND DISCUSSION

Comparative analysis of the subcellular distribution of L- and D-R8–Alexa Fluor® 488

We reported previously on the distinct labelling patterns of L-R8–Alexa Fluor® 488 in the CD34$^+$ leukaemic KG1a cell line when incubations were performed either on ice (referred to as 4 °C) or at 37 °C [11]. As shown in Figure 1(A), confocal microscopy of cells incubated for 1 h at 4 °C with 2 μM L-R8–Alexa Fluor® 488 reveals the peptide to be localized throughout the cell, including the nucleus, and this compares with vesicular labelling only, when identical experiments were performed at 37 °C (Figure 1C). Our ability to label the nucleus of these live cells with the DRAQ5 probe also supports our previous observations showing heterogeneity with respect to the intensity of peptide labelling when peptide incubations are performed at this temperature [11]. To obtain these images, we captured multiple sections through the *z*-axis and then overlaid the data to create a single merged maximum projection image. Each individual section that contributed to form these merged images (Figure 1) is shown in Supplementary Movies 1–4 at http://www.BiochemJ.org/bj/403/bj4030335add.htm.

We performed identical experiments with the D-enantiomer of R8, and, similar to the L-form, the peptide localizes to vesicles at 37 °C (Figure 1D and Supplementary Movie 4). When the cells

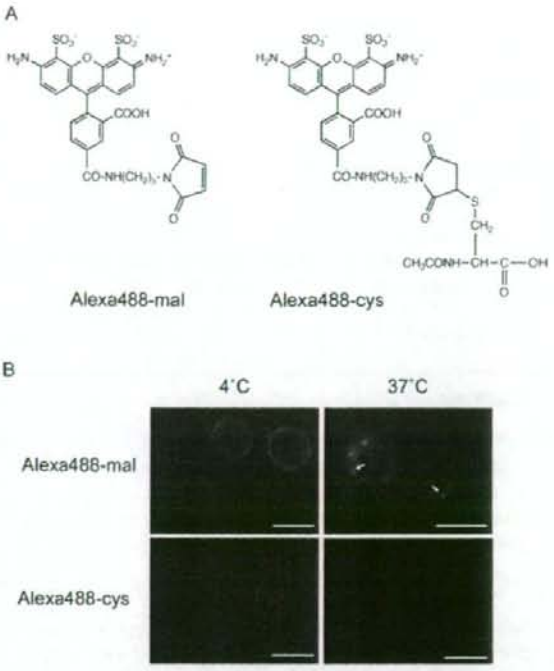

Figure 2 Cellular distribution of activated and inactivated Alexa Fluor® 488–C_5–maleimide

(**A**) Chemical structures of activated (Alexa488-mal) and inactivated Alexa Fluor® 488–C_5–maleimide (Alexa488-cys), following its conjugation to *N*-acetylcysteine. (**B**) Cellular distribution of Alexa488-mal and Alexa488-cys. KG1a cells were incubated with 2 μM label for 1 h at 4 or 37 °C before washing and analysis by fluorescence microscopy. Arrows depict vesicular labelling that was only observed with Alexa488-mal at 37 °C. Scale bars, 10 μm.

were incubated with D-R8–Alexa Fluor® 488 at 4 °C, we observed diffuse labelling that was less apparent in the nucleus, but much more prominent in the nucleolus (Figure 1B). This is especially noticeable in the accompanying movie (Supplementary Movie 2) that also highlights the heterogeneity of peptide labelling at 4 °C, from high to undetectable.

In order to refute the possibility that these effects are caused by extracellular-protease-mediated degradation of the peptide, with resulting release and internalization of free fluorophore, we initially incubated the cells at 4 or 37 °C with the activated Alexa Fluor® 488–C_5–maleimide dye that is used to link to the terminal cysteine of the peptide (Figure 2A). At 4 °C, the fluorescence of this compound was confined to the plasma membrane, and, when identical experiments were performed at 37 °C, intracellular vesicles were also labelled (Figure 2B). However, compared with experiments performed with the equivalent concentrations of L-R8–Alexa Fluor® 488 (Figure 1C), much higher exposure times were required to observe these structures. This suggested that, at both temperatures, the activated dye was conjugating to plasma membrane thiol groups and that these conjugates remained on this structure in the absence of endocytosis at 4 °C, but were internalized at 37 °C. We therefore inactivated the maleimide functional group with *N*-acetylcysteine and observed that even the relatively high exposure times utilized to see the activated dye at 37 °C were not sufficient to label the cells at either temperature (Figure 2B). Thus the fluorescence observed in Figure 1 was a product of R8-mediated delivery to endosomes at 37 °C or to the cytosol, nucleus

© The Authors Journal compilation © 2007 Biochemical Society

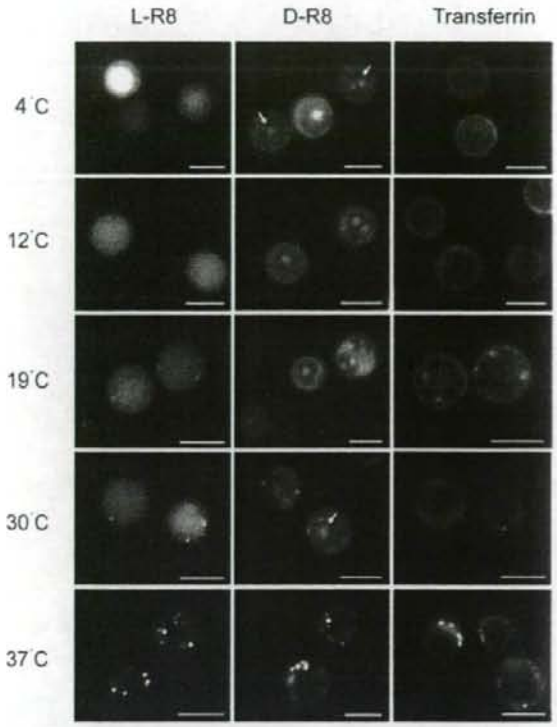

Figure 3 Temperature-dependent cellular distribution of R8–Alexa Fluor® 488 peptides and Alexa Fluor® 488–Tf

KG1a cells were incubated at various temperatures between 4 and 37 °C for 1 h with 2 μM L- or D-R8–Alexa Fluor® 488 or 100 nM Alexa Fluor® 488–Tf before washing and analysis by fluorescence microscopy. Arrows depict labelling of the nucleolus that is unique to D-R8–Alexa Fluor® 488 at up to 30 °C. Scale bars, 10 μm.

and nucleolus at 4 °C. We performed identical experiments with a control peptide NH_2-(Gly-Ser)$_4$-Gly-Cys-(Alexa Fluor® 488)-amide and, at 2 μM, this was undetectable in cells using fluorescence microscopy (results not shown).

Effects of temperature on subcellular distribution and cellular fluorescence profiles for L- and D-R8–Alexa Fluor® 488

Similar microscopy experiments were then performed with L- and D-R8–Alexa Fluor® 488 at temperatures between 4 and 37 °C. Figure 3 shows that L-R8–Alexa Fluor® 488 diffusely labels the entire cell when incubations were performed at $\leqslant$ 19 °C, but, at higher temperatures up to 30 °C, the diffuse fluorescence is accompanied by vesicular labelling. In cells incubated with the D-R8 peptide, there was similar but additional nucleolar labelling at all temperatures up to 30 °C; at 37 °C, cellular labelling of both peptides was confined to vesicular structures.

We also performed the same experiments with Alexa Fluor® 488–Tf, which, at 4 °C, is expected only to bind the Tf receptor at the plasma membrane, but not to be internalized, and, at higher temperatures, will be endocytosed into clathrin-coated vesicles and endosomes [23,24]. As expected, this protein labelled only the plasma membrane at $\leqslant$ 12 °C, but, at higher temperatures, plasma membrane labelling was accompanied by vesicular labelling that increased in intensity as the temperature was increased to 37 °C. Thus these R8-based peptides behaved quite differently from

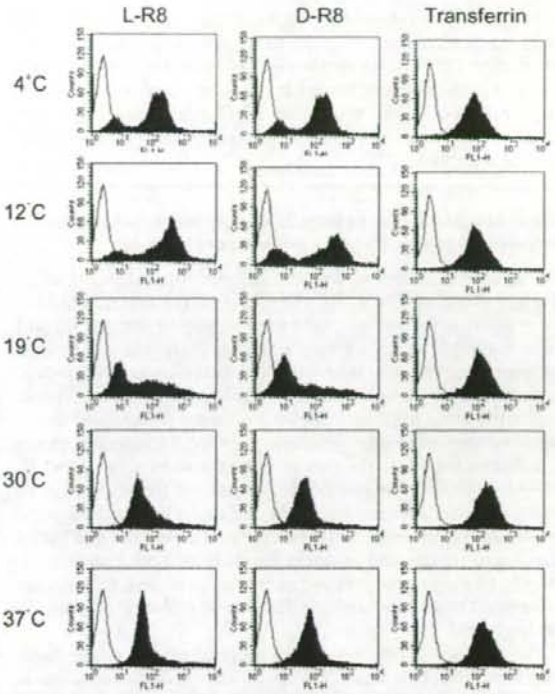

Figure 4 Temperature-dependent cellular fluorescence profiles for R8–Alexa Fluor® 488 peptides and Alexa Fluor® 488–Tf

KG1a cells were incubated at various temperatures between 4 and 37 °C for 1 h with 2 μM L- or D-R8–Alexa Fluor® 488 or 100 nM Alexa Fluor® 488–Tf before washing and analysis by flow cytometry. Unfilled peaks represent untreated cells.

each other and from Tf when they were incubated with cells at temperatures $\leqslant$ 30 °C. The data also suggest that, unlike Tf, the peptides have at least two independent, but temperature-dependent, uptake mechanisms. Similar differences in cellular distribution of peptides Tat P59W, R7 and R7W were also noted in adherent cells when incubations are performed at 4 °C or 37 °C [12,15], thus suggesting that this differential labelling is not a feature unique to these leukaemic cells.

We showed previously using flow cytometry that cellular fluorescence profiles of cells incubated with R8 at 4 °C differ from those incubated at 37 °C [11,14]. We therefore performed flow-cytometric analysis with cells incubated with 2 μM L- and D-R8–Alexa Fluor® 488 at the same selected temperatures between 4 and 37 °C. The results shown in Figure 4 show clear temperature-dependent profiles, but the L- and D-forms gave very similar results. Two peaks were observed for both peptides after 4–12 °C incubations, but, at 19 °C, the lower peak is much more apparent, with a concomitant broadening of the high peak. Only one peak was observed for both peptides when incubated with cells at 30–37 °C.

Again, Alexa Fluor® 488–Tf was used for comparative analysis, and only one fluorescence peak, with the expected increasing intensity with increasing concentration, was observed at all temperatures (Figure 4). For this ligand, the data allow for easy quantification of cell-associated fluorescence, but this is not the case for quantification of cell-associated L- or D-R8–Alexa Fluor® 488 at $<$ 30 °C. This is why the profiles are shown here rather than just the geometric mean values. Interestingly, previous studies in

© The Authors Journal compilation © 2007 Biochemical Society

Jurkat T-cells also showed two peaks of fluorescence, but the cells were incubated with a much higher concentration (12.5 μM) of R9 at 25 °C [25]. In conclusion, the data from this section suggest that endocytosis of peptides and Tf occurs at a reasonably uniform rate throughout the cell population, but that differences exist with respect to the capacity of the cells to associate with the peptides at temperatures < 37 °C.

Effects of concentration on subcellular distribution and cellular fluorescence profiles for L- and D-R8–Alexa Fluor® 488

We then investigated whether the cellular fluorescence profiles that we observed at 4 °C were sensitive to the concentration of the peptides in the medium. Cells were incubated with 0.25–5 μM peptide for 1 h before washing and immediate analysis by flow cytometry or, following the peptide incubations, they were treated further with trypsin and washed with heparin solutions. These additional steps have been shown to reduce plasma membrane labelling that contributes significantly to the fluorescence values in adherent cells [7]. The data in Figure 5 show that L- and D-R8–Alexa Fluor® 488 generated two peaks of fluorescence at all concentrations, irrespective of whether the cells were subjected further to trypsin and heparin treatment. These were designated 'Low' and 'High', and the mean intensity of both generally increased as the peptide concentration was increased; this was accompanied by an increase in the fraction of cells that appeared in the High peak.

Trypsinization appeared to have minimal effects on the fluorescent profiles, but, at > 1 μM, there was a visible reduction in the geometric mean of the low peaks. To analyse this further, the geometric means of the separate peaks at all studied concentrations were quantified, and the results in Table 1 demonstrate that the fluorescences of the Low peaks are significantly reduced ($P < 0.05$) by trypsin/heparin treatment at concentrations $\geqslant 0.5$ μM for L-R8 or $\geqslant 1$ μM for D-R8. However, there was no significant decrease in the fluorescence of the High peak when the peptide concentration was $\geqslant 0.5$ μM, and, even at 0.25 μM peptide concentration, $\geqslant 75$ % of the fluorescence in the High peak fraction was insensitive to trypsin/heparin treatment.

We do not currently have an explanation as to why a particular cell should fall into the Low or High peak population. It is conceivable that the Low peak represents cells with the peptide located within the extracellular matrix of the plasma membrane or even embedded in the lipid bilayer, and that this fraction is only partially sensitive to trypsin and heparin treatment. When cells were incubated for 1 h at 4 °C with L-R8–Alexa Fluor® 488, washed and then incubated for a further 1 h at 4 or 37 °C, there was no significant effect on cellular fluorescence profiles or Low and High peak values (results not shown). The possibility also exists that the loss of the Low peak at higher peptide concentrations is a result of fluorescence quenching and that, for L-R8, fluorescence could be diminished further by proteolysis. This is, however, unlikely, as the intensity of the Low peaks is enhanced with increasing peptide concentrations, but they do not increase in intensity upon trypsinization and heparin washing and neither do they shift to baseline levels. Parallel experiments of peptide association against cell-cycle status may help to define characteristics that predispose the cells to having different capacities to associate with or internalize these peptides.

Fluorescence microscopy was then utilized to determine whether increasing the peptide concentration from our standard 1–2 μM affected the subcellular labelling pattern when incubations were performed at 37 °C. Cells were therefore incubated with 2–10 μM peptide for 1 h, washed and then analysed. Figure 6(A) shows that increasing the concentration from 2 to only 5 μM

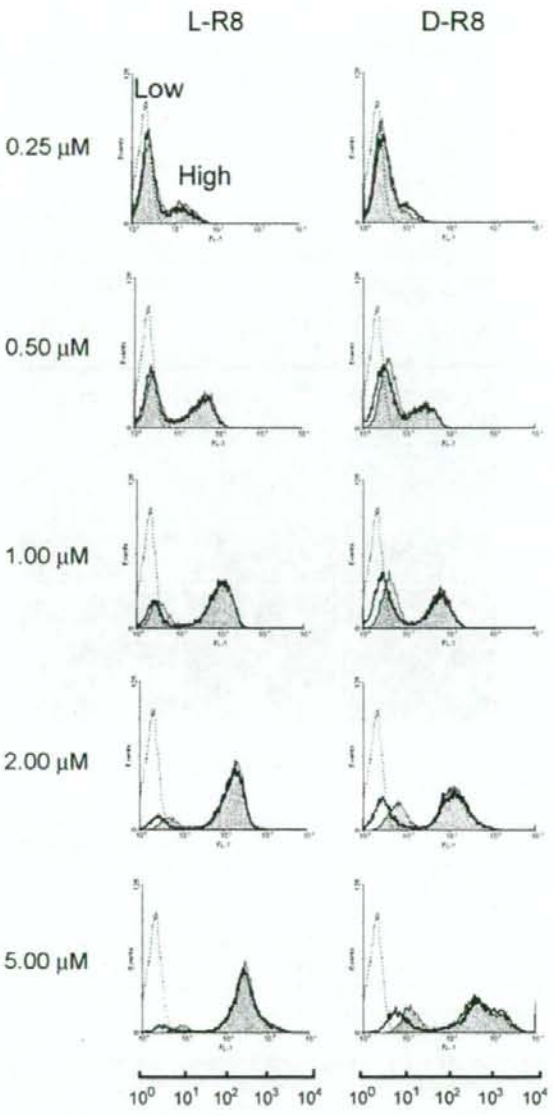

Figure 5 Concentration-dependent cellular fluorescence profiles for R8–Alexa Fluor® 488 peptides

KG1a cells were incubated for 1 h with 0.25–5.0 μM L- or D-R8–Alexa Fluor® 488 at 4 °C. The cells were then washed and either immediately analysed by flow cytometry (filled grey) or were treated further with trypsin and heparin before analysis (unfilled peaks). Broken lines represent untreated cells. In all experiments performed at 4 °C, two peaks of fluorescence of varying intensities were obtained, and were designated Low and High. The geometric mean values of the two designated peaks were calculated for all conditions, and these were combined with results from repeat experiments to generate Table 1.

resulted in a dramatic increase in the fraction of the peptide that was localized to the cytosol. Vesicular labelling was still evident at this higher concentration, up to 10 μM, but this was somewhat masked by the strong diffuse labelling. In cells incubated with 10 μM D-R8–Alexa Fluor® 488, the nucleolus was also prominently labelled, but L-R8–Alexa Fluor® 488 failed to label these structures even at these higher concentrations. In all of our

© The Authors Journal compilation © 2007 Biochemical Society

Table 1 Analysis of fluorescence peaks obtained from incubating cells with increasing concentrations of R8–Alexa Fluor® 488 peptides

KG1a cells were incubated with 0.25–5.0 μM L- or D-R8–Alexa Fluor® 488 for 1 h at 4 °C. The cells were then washed and either immediately analysed by flow cytometry (PBS) or treated further with trypsin and heparin before analysis (trypsin/heparin). Two peaks of fluorescence were observed and designated Low and High (Figure 5). Shown are the geometric mean values for the Low and High peaks for all depicted concentrations. Results are means ± S.D. for two individual experiments performed in duplicate. Statistical analysis for comparing the geometric means of untreated compared with treated fluorescence cells was performed using Student's *t* test. *$P < 0.05$; decreased relative to PBS control.

(a) L-R8

	Low		High	
Peptide concentration (μM)	PBS	Trypsin/heparin	PBS	Trypsin/heparin
0.25	2.76 ± 0.14	2.78 ± 0.45	17.20 ± 0.45	16.10 ± 0.26*
0.50	3.12 ± 0.13	2.94 ± 0.12	39.99 ± 3.27	37.87 ± 2.35
1.00	3.89 ± 0.23	3.16 ± 0.22*	98.88 ± 4.60	93.64 ± 2.74
2.00	4.78 ± 0.28	3.51 ± 0.19*	175.14 ± 10.61	165.90 ± 14.05
5.00	9.44 ± 1.21	4.69 ± 0.47*	357.73 ± 62.42	338.55 ± 46.47

(b) D-R8

	Low		High	
Peptide concentration (μM)	PBS	Trypsin/heparin	PBS	Trypsin/heparin
0.25	3.18 ± 0.12	2.94 ± 0.19	15.73 ± 1.27	12.46 ± 0.57*
0.50	4.09 ± 0.18	3.07 ± 0.05*	28.71 ± 5.20	30.77 ± 4.56
1.00	4.80 ± 0.51	3.17 ± 0.17*	83.14 ± 19.10	76.78 ± 17.98
2.00	6.07 ± 0.17	3.82 ± 0.28*	147.86 ± 16.75	155.025 ± 13.61
5.00	11.83 ± 1.69	6.18 ± 1.05*	430.48 ± 63.94	521.81 ± 105.11

experiments, we were unable to observe the presence of L-R8–Alexa Fluor® 488 in the nucleolus, but clear nucleolar labelling was observed when cells, incubated with 2 μM peptide at 4 or 37 °C, were fixed with paraformaldehyde before microscopical analysis (Figure 6B, and results not shown).

These data strongly suggest that endocytosis as an uptake mechanism, and visible by fluorescence microscopy, is only dominant to a specific peptide concentration. At levels higher than this threshold, the peptide also enters cells by an alternative mechanism. It is highly unlikely that this very strong cytoplasmic labelling at 5–10 μM is caused by endocytosis and then translocation from the endo/lysosomal system, as similar data were obtained when the peptide incubations were reduced to 10 min (Figure 6C). Vesicular labelling in these shorter incubations was, however, less pronounced. Equally, it is unlikely that at low peptide concentrations at 37 °C that translocation from cytosol to endosomes and lysosomes is significant, as incubations performed at 4 °C in the presence of peptide, followed by 37 °C incubations without peptides, had no effects on the pattern of labelling (results not shown).

At concentrations $\geqslant 5$ μM, it is conceivable that some of the observed effects were due to peptide-induced membrane damage and cytotoxicity. Parallel experiments were therefore performed in cells incubated with 10 μM L- or D-R8–Alexa Fluor® 488 and PI (propidium iodide), which would only be expected to enter dead or leaky cells. There was no increase in PI-labelled cells under these conditions (results not shown) and longer 24 h cell-viability assays demonstrated that D- and L-peptides lacked significant toxicity up to 12.5 μM (Figure 6D).

The majority of studies investigating the uptake mechanisms of CPPs have also utilized peptide concentrations between 0.5 and 10 μM; however, the universality of these effects with respect to other types of cells remains to be determined. There are likely to be different threshold concentrations for different cell lines, as each will have their unique repertoire of plasma membrane lipids, proteins and their associated carbohydrates. These may all affect the degree of peptide association with molecules protruding from the plasma membrane and/or with molecules localized within the bilayer itself.

Effects of cholesterol depletion on subcellular distribution of L- and D-R8–Alexa Fluor® 488

As translocation across membranes was occurring at higher concentrations of peptide, we investigated whether this process could be promoted at lower concentrations by perturbing the organization of the plasma membrane. For this, we depleted plasma membrane cholesterol using a standard method employing the cholesterol-sequestering agent MβCD [26]. Cells were pre-treated with 5 mM MβCD for 30 min before the addition of 2 μM L- or D-R8–Alexa Fluor® 488 for 1 h at 37 °C and immediate analysis by fluorescence microscopy. MβCD-treated cells had strong diffuse labelling of the cytoplasm and nucleus, with very little evidence of vesicular uptake; consistent with our previous experiments, nucleolar labelling was unique to the D-form (Figure 7).

Very different results were obtained when parallel experiments were performed with Alexa Fluor® 488–Tf, and, in the present study, cholesterol sequestration completely inhibited vesicular uptake and only the plasma membrane was labelled. MβCD was shown previously to significantly inhibit uptake of Tat peptide [9] and penetratin in a number of cell lines [27], suggesting that uptake is occurring via plasma membrane domains called rafts. These are enriched in cholesterol [28], and MβCD is often used to discriminate between uptake via clathrin-coated pits and raft-dependent pathways [29]. Studies in a number of adherent cell lines have, however, shown that Tf internalization is inhibited (40–60 %) in MβCD-treated cells [30]. Thus the widespread use of MβCD and other cholesterol-depleting agents should be treated with caution unless control experiments with ligands for clathrin-mediated uptake and other pathways are also investigated. Our experiments raise the interesting possibility that the organization of the plasma membrane into cholesterol-enriched lipid rafts inhibits plasma membrane translocation. They also suggest that the normal site of entry of the peptides, especially at low temperatures, may be the more fluidic regions of the plasma membrane containing less cholesterol.

At 2 μM, D-R8–Alexa Fluor® 488, unlike L-R8–Alexa Fluor® 488, labelled the nucleolus at all temperatures up to 30 °C, but this was also observed when the peptide concentration was increased

© The Authors Journal compilation © 2007 Biochemical Society